Modeling of the transient behavior of a slurry bubble column reactor for CO_2 methanation, and comparison with a tube bundle reactor

Jonathan Lefebvre [a, *], Siegfried Bajohr [a], Thomas Kolb [a, b]

[a] Karlsruhe Institute of Technology, Engler-Bunte-Institut, Fuel Technology, Engler-Bunte-Ring 1, 76131, Karlsruhe, Germany
[b] DVGW Research Center at Engler-Bunte-Institut, Engler-Bunte-Ring 3, 76131, Karlsruhe, Germany

A B S T R A C T

In this publication, the performance of a slurry bubble column reactor (SBCR) and a tube bundle reactor (TBR) are compared for steady state and transient Power to Gas (PtG) operation. Transient PtG conditions are modeled using gas load step changes between 25 and 100% of the reactor maximum capacities in 1 s.

For steady state operation the TBR facilitates much higher gas hourly space velocities (*GHSV*) as compared to the SBCR. A sensitivity analysis shows that the TBR is limited by heat transfer, while the SBCR is limited by gas/liquid mass transfer.

For transient PtG operation the TBR undergoes significant temperature changes within a short time resulting in out of specification product gas qualities and unacceptable temperature hot spots; the SBCR temperature shows marginal changes upon transient operating conditions, and the outlet gas composition sticks to the gas quality requirements.

Finally, measures to improve the efficiency of both reactors are proposed considering dimensionless numbers. The *GHSV* of the SBCR can be enhanced by increasing the specific interfacial area controlling gas/liquid mass transfer, while the transient behavior of the TBR can be improved by reducing the catalyst concentration/activity or by mixing the catalyst with high heat capacity inert material in detriment of the *GHSV*.

Keywords:
CO_2 methanation
Slurry bubble column reactor
Tube bundle reactor
Steady-state modeling
Transient modeling
Power-to-Gas

1. Introduction

With the COP21 Agreement, the parties of the United Nations Framework Convention on Climate Change agreed on reducing greenhouse gas emissions in order to hold the increase in global average temperature well below 2 K [1]. To achieve this goal, CO_2 emissions from human activities have to be reduced drastically. Especially, CO_2 from fossil fuels must be reduced through a drastic increase of the share of renewable and environmentally friendly energy sources such as wind and solar power in energy systems. However, the current share of electricity in final energy consumption is relatively low, e.g. about 22% in the EU. The remaining energy demand required for industrial applications, mobility and heating must be covered by other forms of energy like chemical energy carriers, in order to avoid a large and costly extension of the existing power grid. The Power to Gas (PtG) process, which transforms electrical energy into storable chemical energy can be used to connect the power grid to the natural gas grid with all its established transportation, storage and utilization applications. In a PtG process chain water electrolysis with subsequent catalytic methanation of the intermediate hydrogen with carbon dioxide can be used for the production of synthetic natural gas (SNG) (see Eq. (1)) [2–5].

$$CO_2 + 4\ H_2 \rightleftharpoons CH_4 + 2\ H_2O \quad \Delta h_r^{\theta} \qquad 165\ \mathrm{kJ/mol} \qquad (1)$$

In order to exploit all the benefits of the PtG technology foremost the time scale decoupling of renewable energy supply and final energy utilization the methanation step involved in the PtG process has to be a transient process. Ronsch et al. [6] have already shown that adiabatic fixed bed reactors with interstage cooling and gas recirculation, which are state of the art steady state reactors for commercial CO methanation plants, have thermal runaway issues when they are operated under transient conditions.

Hence, new reactor concepts are required for the PtG process. The current benchmark PtG facility in Werlte (Germany) uses a tube

* Corresponding author.
E-mail address: jonathan.lefebvre@kit.edu (J. Lefebvre).

bundle reactor (TBR, see Fig. 1) for catalytic methanation of CO_2 from a biogas plant [7]. However, the literature related to this fa cility is scarce and little information is available regarding the transient behavior of this reactor. A slurry bubble column reactor (SBCR, see Fig. 2) represents a promising alternative to fixed bed technology. The advantages of a SBCR are the high heat capacity of the slurry phase as well as the excellent mixing in the reactor, which results in well controlled, almost uniform temperature profile even under transient operating conditions [8].

The aim of this study was to identify the potential of a SBCR as methanation reactor integrated in a PtG process chain. In this publication the design of a SBCR and a STFR for catalytic CO_2 methanation was established and discussed based on steady state simulations.

2. Literature review on reactor modeling

In the following, a literature review was performed on the recent publications related to SBCR and fixed bed reactor modeling.

2.1. Slurry bubble column reactor

Basha et al. [9] differentiate three types of bubble column reactor (BCR) and SBCR models: axial dispersion models (ADM), multiple cell circulation models (MCCM), and computational fluid dynamics (CFD) models. Most of the SBCR models available in the literature are ADM that have been developed for Fischer Tropsch synthesis (FTS) application.

In ADM integral parameters known as axial dispersion co efficients $D_{i,ax}$ are used to describe the different mixing behaviors within the three phases involved in a SBCR. These axial dispersion coefficients are implemented in the partial differential equations describing a SBCR (see e.g. Eq. (6)). Some authors chose to simulate SBCR assuming ideal reactor behavior. Often, the gas phase is treated as a PFR ($D_{i,ax}$ 0), while the slurry phase is described as CSTR ($D_{i,ax}$ ∞) [10–20]. Other authors implemented axial dispersion coefficients from correlations available in the literature, as ideal reactor behavior is not able to represent correctly the real phase mixing within SBCR [21–28].

In MCCM a BCR [29–41] or a SBCR [42,43] is divided into several cells with defined mixing behavior, e.g. assuming a better mixing in the bottom and the top of the liquid phase as compared to the rest

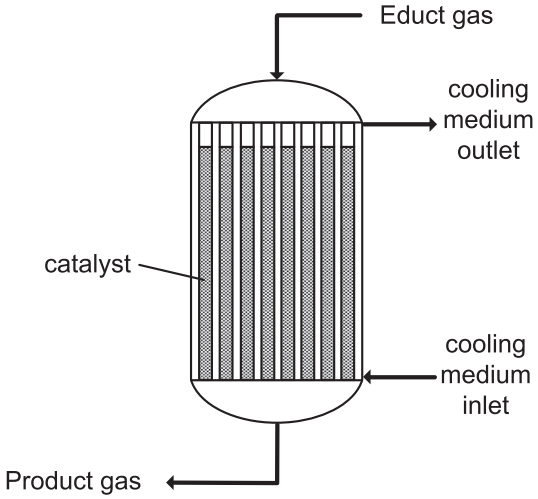

Fig. 1. Scheme of a tube bundle reactor.

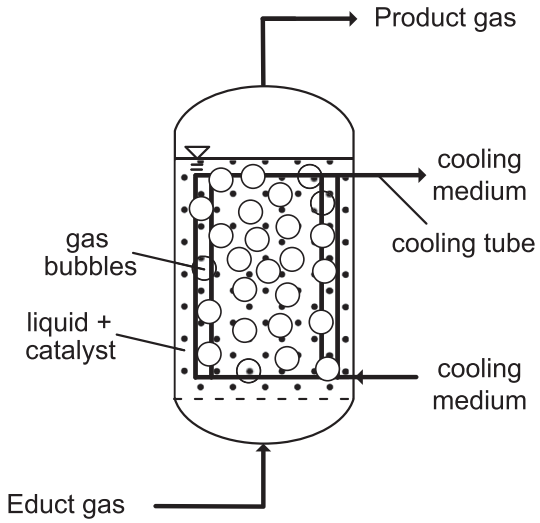

Fig. 2. Scheme of a slurry bubble column reactor.

of the reactor. MCCM require the detailed knowledge of cell num ber as well as cell mixing behavior. However, these data are experimentally hard to measure and to verify, and therefore scarce in literature [9].

CFD models can provide more detailed SBCR modeling through consideration of the fluid dynamics of the three phases. Two ap proaches for CFD modeling have been made so far: the Euler Euler approach (gas and liquid are treated as fluid, solid are assumed as fluid or uniformly distributed) [44–64] and the Euler Lagrange approach (gas is treated as fluid or particle, liquid is assumed as fluid, and solid is treated as particle) [65–71]. Nevertheless, the later approach is usually not suited for the simulation of a whole SBCR, as CPU time is extremely high. This is the reason why the Euler Euler approach is usually preferred. CFD models require drag coefficient models to simulate the flow fields inside a SBCR. How ever, drag coefficient models for two and three phase systems are scarce and usually not applicable, because coalescence and break up of gas bubbles in BCR/SBCR are still not well understood [9].

Simulation of SBCR was performed for transient FTS operation [8,25,28]. For these simulations, de Swart et al. [8] and Rados et al. [25] used an ADM operating in the heterogeneous flow regime. They considered the flow of large gas bubbles as PFR, while they assumed the small gas bubbles to follow the slurry phase flow. Solid particles were either uniformly distributed in the reactor [25] or the solid concentration was assumed to follow an exponential decay with increasing reactor height [8]. The authors concluded that SBCR are suited for transient FTS, as they do not undergo thermal runaway. Nevertheless, they emphasized the need for ac curate investigation of the liquid phase backmixing in SBCR.

In this publication, the transient behavior of the SBCR for CO_2 methanation was simulated with a model based on the ADM of Rados et al. [25].

2.2. Tube bundle reactor

Fixed bed reactors are state of the art. As such a large number of fixed bed reactor models have been developed. In this work, only the recent publications related to fixed bed reactors for catalytic CO_2 methanation were reviewed.

Fixed bed reactor models can be classified into homogeneous and heterogeneous models [72]. Homogeneous models neglect local concentration and temperature difference between the

catalyst and the gas phase. This assumption is valid when there is no mass or heat transfer limitation within the reactor. These limi tations are usually estimated with the Mears' and Anderson's criteria [73,74] as well as the Thiele modulus [75] (see Appendix A and B). If these criteria are not fulfilled, concentration or temper ature differences are expected between the catalyst and gas phase. In this case, heterogeneous models are to be considered. These models treat each phase separately, i.e. concentrations and tem perature in the catalyst particle are different from the concentra tions and temperature of the bulk gas phase. These models offer a higher degree of precision but require much higher CPU time, as the number of partial differential equations is doubled.

Fixed bed reactor models can be further categorized into one dimensional (1D) and two dimensional (2D) models [72]. 1D models do not consider any gradients along the radial axis of the reactor. However, as the temperature of fixed bed reactors may be controlled by a heat exchanger at the reactor tube wall, radial temperature and concentration gradients may be observed in these reactors. 2D models consider these radial gradients and describe the evolution of concentration and temperature along the vertical and radial axes. Though 2D models offer more detailed results as compared to 1D models, they need much higher calculation times, as computers must solve partial differential equations with two spatial coordinates.

Schlereth et al. [76] investigated the influence of model types on the simulation results of a steady state fixed bed reactor for CO_2 methanation. They investigated 1D and 2D homogeneous models as well as a 1D heterogeneous model. They showed that simple 1D homogeneous models are able to describe qualitatively the behavior of a methanation fixed bed reactor. However, 2D homo geneous models are better suited for detailed and quantitative description of methanation reactors.

Even more recently, Sun et al. [77,78] investigated the transient behavior of a fixed bed reactor for CO_2 methanation using a 1D homogeneous reactor model. Attention was not paid to dynamic operation but to catalyst deactivation over time.

In this publication, the transient behavior of the TBR was modeled with a 1D homogeneous model. A 2D homogeneous model was also prepared but resulted in excessive calculation times.

3. Reactor modeling

The SBCR and the TBR were designed to reach a CO_2 conversion of 0.9 at 20 bar with a feed gas composition $H_2/CO_2/CH_4$ of 4/1/1 at a volume flow rate of 900 m^3/h (STP) under steady state operation. These process parameters correspond to a medium size biogas fermenter of 300 m^3/h (STP) biogas output. The feed gas compo sition is representative of a typical biogas composition with a CO_2/CH_4 ratio of 1, which is enriched by H_2 for complete CO_2 conversion to CH_4. All relevant input parameters for the two reactor models are summarized in Table 1.

In this work, the response of the SBCR and TBR for transient CO_2 methanation was simulated for very fast inlet gas velocity changes taking place within 1 s. This situation aims to represent a PtG fa cility responding to a sudden surplus of renewable electricity if no H_2 buffer tank is integrated. This situation represents a worst case scenario, as the volume of pipings and intermediate devices are neglected. The aim of this study was to assess the evolution of reactor temperature and outlet gas quality resulting from the gas velocity change.

The following gas load changes were considered to model this situation:

Table 1
Input parameters for the two reactor models.

Parameter	Value
$V_{in,STP}$	900 m^3/h
p	20 bar
$y_{H_2,in}$	4/6
$y_{CO_2,in}$	1/6
$y_{CH_4,in}$	1/6
ρ_S	1050 kg/m^3
$c_{p,S}$	1000 J/(kg·K)
λ_S	0.2 W/(m·K)
ε_S	0.4

1. From 25 to 50% of the maximum methanation reactor capacity, i.e. 25% load in 1 s;
2. From 50 to 100% of the maximum methanation reactor capacity, i.e. 50% load in 1 s;
3. From 75 to 100% of the maximum methanation reactor capacity, i.e. 25% load in 1 s;
4. Reverse load changes for each of the three above mentioned load changes.

Harsh gas load changes are usually not performed on TBR, as they are sensitive to a change in superficial gas velocity. In practice, a well defined and mild change over time of gas velocity and cooling medium temperature is implemented. However, this means that an expensive H_2 tank is required to buffer the H_2 volume flow rate from the electrolyzer. Gotz et al. [79] have shown that it is more economical to operate a methanation reactor under transient operating conditions as compared to build a H_2 buffer tank. Consequently, the worst case scenario in terms of gas load change without H_2 buffer tank was considered in this work. A minimum gas load corresponding to 25% of the maximum reactor capacity is assumed, as lower gas loads would lead to a change in SBCR hy drodynamic regime which is not considered in the SBCR model.

Both reactor models were implemented in Matlab® R2015a using an ode15s solver with a relative and absolute tolerance of 0.1%. The time step increment was set to 1 s. A sufficiently long period of time was simulated in order to reach steady state. In the following a detailed description of the SBCR and TBR model is given.

3.1. Slurry bubble column reactor model

3.1.1. Model structure

The ADM model for SBCR is schematically represented in Fig. 3. This model uses axial dispersion coefficients for the gas and liquid phase $D_{G,ax}$ and $D_{L,ax}$, respectively, and considers two bubble classes, "small" and "large", assuming that large bubbles flow up wards as a PFR, while small bubbles recirculate with the liquid phase entrained by the large bubble flow. The gas holdup ε_G, i.e. the relative gas phase volume in the reactor, is therefore divided into large bubbles ($\varepsilon_{G,large}$) and small bubbles ($\varepsilon_{G,small}$). Mass transfer takes place between the bubbles and the slurry phase and depends on the volumetric gas/liquid mass transfer coefficient $k_L a_i$ and the dimensionless Henry's law constant $H_{i,cc}$ of a gas species i. The chemical reaction takes place at the surface of the catalyst, while the heat exchange takes place between the slurry phase and an internal cooling surface area which is equally distributed along the reactor. The external heat transfer, i.e. on the cooling medium side, is neglected and the cooling medium temperature is set constant.

The SBCR was simulated under the heterogeneous flow regime in order to allow for a high gas hourly space velocity (*GHSV*, see Eq. (2)). The reactor was operated as semi batch reactor, i.e. no fresh or

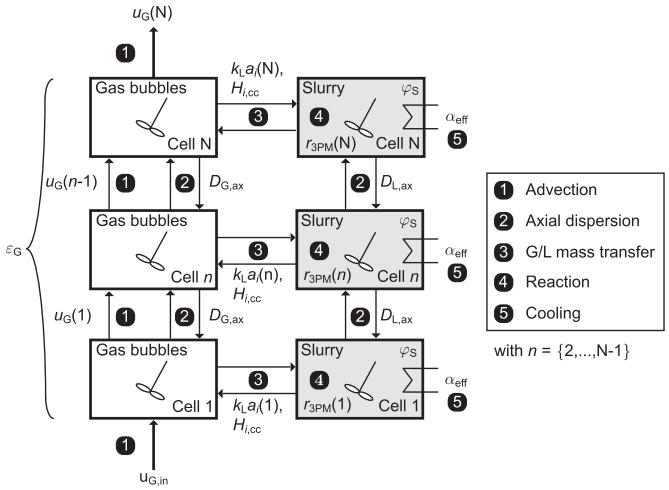

Fig. 3. Structure of the slurry bubble column reactor model, including the parameters influencing the mass and heat transfer phenomena.

recycled slurry was circulated in the reactor (u_L 0 m/s). Only the gas phase flowed through the SBCR. A perforated plate, which was designed based on previous hydrodynamic measurements [80,81], was used as gas sparger.

$$GHSV \quad \frac{\dot{V}_{in,STP}}{V_R} \tag{2}$$

3.1.2. Model assumptions

The SBCR model incorporates the following assumptions. As sumptions 1 to 4 are illustrated in Fig. 4.

1. Gas phase is assumed ideal and Raoult's law can be applied, i.e. $c_{i,G}$ $p_i/(RT)$;
2. Mass transfer resistance between the gas and liquid phase is located in the liquid phase only, i.e. the gas concentration at the G/L interphase $c^*_{i,G}$ equals the gas concentration in the bulk gas phase $c_{i,G}$;
3. Gas/liquid equilibrium is reached for each gas species, i.e. Henry's law expressed in Eq. (3) is applicable at the gas/liquid interphase;

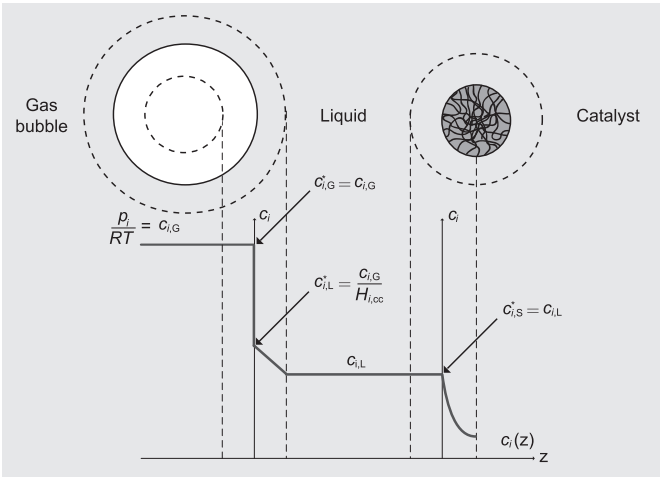

Fig. 4. Concentration profile of an educt gas species along the three phases of the slurry bubble column reactor model.

4. Mass transfer resistance between the liquid phase and solid phase (catalyst) is neglected, i.e. the gas concentration at the L/S interphase $c^*_{i,S}$ equals the gas concentration in the bulk liquid phase $c_{i,L}$;
5. There is no radial concentration and temperature gradient, i.e. the reactor is discretized only in the vertical direction z (1D model);
6. Catalyst is uniformly distributed in the liquid phase, i.e. $v\varphi_S/vz$ 0.
7. There is no direct contact between the catalyst and the gas phase, i.e. no reaction in the gas phase;
8. The three phases are in thermal equilibrium, i.e. $T_G(z)$ $T_L(z)$ $T_S(z)$ $T(z)$;
9. The gas phase is neglected in the energy balance, i.e. $\sum_j \rho_j, c_{p,j}, T$ $\rho_{SL}, c_{p,SL}, T$.

Model assumptions are discussed in the supplementary materials.

3.1.3. Mole and energy balance

With these assumptions, the mole and energy balances around the SBCR can be written as shown in Eqs. (6)–(10). Hereby, the dimensionless Henry's law constant $H_{i,cc}$ describes the concentra tion of gas species i dissolved in the liquid phase $c^*_{i,L}$ (see Eq. (3)).

$$H_{i,cc} \quad \frac{c_{i,G}}{c^*_{i,L}} \quad H_{i,pc}, \frac{1}{R,T} \tag{3}$$

The superficial velocity of small bubbles $u_{G,small}$ is defined in Eq. (4),

$$u_{G,small} \quad \frac{\varepsilon_{G,small}}{\varepsilon_G}, u_G \tag{4}$$

while the superficial velocity of large bubbles is defined in Eq. (5).

$$u_{G,large} \quad u_G \quad u_{G,small} \tag{5}$$

Mole balance for a gas species i in the large bubbles (Eq. (6)):

$$\underbrace{\frac{v}{vt}\left(\varepsilon_{G,large}, c_{i,G,large}\right)}_{\text{Accumulation}} \quad \underbrace{\frac{v}{vz}\left(\varepsilon_{G,large}, D_{G,ax,large}, \frac{vc_{i,G,large}}{vz}\right)}_{\text{Axial dispersion}}$$

$$\underbrace{\frac{v}{vz}\left(u_{G,large}, c_{i,G,large}\right)}_{\text{Advection}} \quad \underbrace{k_L a_{i,large}, \left(\frac{c_{i,G,large}}{H_{i,cc}} \quad c_{i,L}\right)}_{\text{G/L mass transfer}} \tag{6}$$

Mole balance for a gas species i in the small bubbles (Eq. (7)):

$$\underbrace{\frac{v}{vt}\left(\varepsilon_{G,small}, c_{i,G,small}\right)}_{\text{Accumulation}} \quad \underbrace{\frac{v}{vz}\left(\varepsilon_{G,small}, D_{G,ax,small}, \frac{vc_{i,G,small}}{vz}\right)}_{\text{Axial dispersion}}$$

$$\underbrace{\frac{v}{vz}\left(u_{G,small}, c_{i,G,small}\right)}_{\text{Advection}} \quad \underbrace{k_L a_{i,small}, \left(\frac{c_{i,G,small}}{H_{i,cc}} \quad c_{i,L}\right)}_{\text{G/L mass transfer}} \tag{7}$$

Mole balance around the whole gas phase, i.e. small and large bubbles together (Eq. (8)):

$$\underbrace{\frac{\partial}{\partial t}(\varepsilon_G \cdot c_G)}_{\text{Accumulation}} \quad \underbrace{\frac{\partial}{\partial z}(u_G \cdot c_G)}_{\text{Advection}} \quad \underbrace{\sum k_L a_i \cdot \left(\frac{c_{i,G}}{H_{i,cc}} \quad c_{i,L}\right)}_{\text{G/L mass transfer}} \tag{8}$$

Mole balance for a gas species i in the slurry phase (Eq. (9)):

$$\underbrace{\frac{\partial}{\partial t}(\varepsilon_{SL} \cdot c_{i,L})}_{\text{Accumulation}} \quad \underbrace{\frac{\partial}{\partial z}\left(\varepsilon_{SL} \cdot D_{SL,ax} \cdot \frac{\partial c_{i,L}}{\partial z}\right)}_{\text{Axial dispersion}}$$

$$\underbrace{+k_L a_{i,large} \cdot \left(\frac{c_{i,G,large}}{H_{i,cc}} \quad c_{i,L}\right) + k_L a_{i,small} \cdot \left(\frac{c_{i,G,small}}{H_{i,cc}} \quad c_{i,L}\right)}_{\text{G/L mass transfer}} \underbrace{+\nu_i \cdot \eta_{cat} \cdot \varphi_S \cdot \rho_S \cdot r_{3PM}}_{\text{Reaction}} \tag{9}$$

Slurry phase energy balance (Eq. (10)):

$$\underbrace{\rho_{SL} \cdot c_{p,SL} \cdot \varepsilon_{SL} \cdot \frac{\partial T}{\partial t}}_{\text{Accumulation}} \quad \underbrace{\frac{\partial}{\partial z}\left(\varepsilon_{SL} \cdot \lambda_{SL,eff} \cdot \frac{\partial T}{\partial z}\right)}_{\text{Axial dispersion}}$$

$$\underbrace{+\eta_{cat} \cdot \varphi_S \cdot \rho_S \cdot r_{3PM} \cdot (\quad \Delta h_r)}_{\text{Reaction heat}} \underbrace{\alpha_{eff} \cdot a_{cool} \cdot (T \quad T_{cool})}_{\text{Cooling}} \tag{10}$$

The slurry holdup ε_{SL} is defined in Eq. (11),

$$\varepsilon_{SL} \quad \frac{V_S + V_L}{V_R} \quad 1 \quad \varepsilon_G \tag{11}$$

while the effective slurry heat conductivity $\lambda_{SL,eff}$ is defined in Eq. (12).

$$\lambda_{SL,eff} \quad \rho_{SL} \cdot c_{p,SL} \cdot D_{SL,ax} \tag{12}$$

3.1.4. Hydrodynamics and mass transfer

The gas holdups ε_G, $\varepsilon_{G,large}$ and $\varepsilon_{G,small}$ in Eq. (6) to Eq. (8) were calculated with the correlation developed by Behkhish et al. [82], while the volumetric mass transfer coefficients $k_L a_{i,large}$ and $k_L a_{i,small}$ in Eq. (6) to Eq. (8) were calculated with the correlation developed by Lemoine et al. [83]. These correlations were chosen because they were the only available correlations that cover the relevant range of three phase methanation operating conditions.

It is well known that correlations for SBCR dispersion co efficients available in the literature were validated for bubble col umns without solid phase and for small reactor diameter (<0.2 m) and are less relevant for technical SBCR [84–91]. Nevertheless, dispersion coefficients are necessary, because fully ideal reactor models (PFR or CSTR) are not suitable to represent technical SBCR [8,26]. The axial dispersion coefficient correlation developed by Deckwer and Buckhart [91] was implemented in this publication to calculate the axial dispersion coefficients of the small bubbles $D_{G,ax,small}$ and the slurry phase $D_{SL,ax}$, as it is often applied in the literature to model SBCR for FTS [8,26]. The axial dispersion coef ficient of the large bubbles $D_{G,ax,large}$ was set to 0, as the behavior of these bubbles is considered as PFR.

The decrease in superficial gas velocity along the reactor height due to chemical reaction was calculated by solving Eq. (8).

3.1.5. Reaction rate

The intrinsic reaction rate r_{3PM} was calculated using a kinetic rate equation based on the measurements shown in Ref. [92], while the catalyst efficiency was calculated through estimation of the Thiele modulus (see Eqs. (27) and (28) in the Appendix).

3.1.6. Heat transfer

The effective heat transfer coefficient α_{eff} was calculated with a correlation developed by Deckwer et al. [93], as the SBCR modeled in this publication operates within the validity range of Deckwer's correlation. The volumetric heat exchanger surface area a_{cool} was set to 10 m^2/m^3, which is an average value of volumetric heat exchanger surface areas suggested by de Swart et al. [8]. Consid ering the reactor design calculated in section 4.1.1, a_{cool} of 10 m^2/m^3 corresponds to 10 cooling tubes of outer diameter 0.03 m vertically placed inside the SBCR. These cooling tubes occupy less than 8% of the reactor volume.

The slurry properties (density, viscosity, heat capacity and conductivity as well as gas diffusion coefficient) were calculated with Eq. (42) to Eq. (46) in the Appendix, as the validity range of these correlations covers the CO_2 methanation operating condi tions. The liquid used in the SBCR is dibenzyltoluene as it proved to be a suitable liquid for three phase methanation. The maximum allowed temperature for DBT is 350 °C. As CO_2 methanation ex periments were carried up to a maximum temperature of 320 °C [92], the SBCR was designed for an average slurry temperature of 320 °C. Pure dibenzyltoluene properties (viscosity, surface tension, density and heat capacity) can be found in Appendix D and in Ref. [92].

3.1.7. Numerical procedure

In the Matlab® ode15s solver, Eq. (8) to Eq. (10) were solved with the method of lines (MOL), i.e. the partial differential equa tions (PDE) along the vertical axis were discretized, while the solver integrated the ordinary differential equations (ODE) along time. The reactor was discretized in N 100 cells resulting in 13×100 1300 ODE. For a number of cells larger than 100, modeling results did not vary significantly from the N 100 case (see Fig. 18 in the supplementary materials).

3.1.8. Reactor design strategy

To simplify the design of a methanation SBCR, several boundary conditions had to be fixed. These boundary conditions as well as their justification are listed in Table 2.

In order to reach a CO_2 conversion of 0.9 and a mean slurry temperature $\overline{T}_{SL}$ of 320 °C (see definition in Eq. (13)), three pa rameters could be adjusted: the catalyst concentration φ_S, the reactor height h_R and the cooling medium temperature T_{cool}. The following strategy was used to achieve the desired CO_2 conversion and reactor temperature. First, φ_S, h_R and T_{cool} were guessed and the Matlab® model solved the PDE and delivered a result. If the resulting CO_2 conversion and the mean slurry temperature were

Table 2
Slurry bubble column reactor boundary conditions.

Parameter	Value	Justification
$\overline{T}_{SL}$	320 °C	Derived from own experiments (see Ref. [92])
$T_{SL,max}$	350 °C	Taken from DBT safety data sheet [99]
$T_{G,in}$	$\overline{T}_{SL}$	Reduction of reactor variables
d_P	$75,10^{-6}$ m	Derived from own experiments (see Ref. [92])
d_{hole}	$1,10^{-4}$ m	Derived from previous experiments [80]
a_{free} $1-\frac{A_{hole}}{A_{gas\ sparger}}$	$7.2,10^{-3}$	Derived from previous experiments [80]
N_{hole}	83095	Derived from a_{free} and d_{hole}
$u_{G,in,max}$	0.3 m/s	Taken from literature [100]
d_R	0.34 m	Derived from $u_{G,in,max}$ and $V_{G,in,STP}$
a_{cool}	10 m^2/m^3	Taken from literature [8]

not satisfying, φ_S, h_R and T_{cool} were iteratively varied until the desired CO_2 conversion and mean slurry temperature were ach ieved. This algorithm is illustrated in Fig. 32 in the supplementary materials.

$$\overline{T}_{SL} \quad \frac{1}{h_R}\int_0^{h_R} T_{SL}(z)dz \tag{13}$$

3.2. Tube bundle reactor model

3.2.1. Model structure

The TBR was modeled as a 1D homogeneous tube bundle reactor which is schematically represented in Fig. 5. The educt gases enter at the top of the reactor tubes and react along the reactor at the catalyst surface. Each reactor tube is cooled by the cooling medium with a constant temperature T_{cool}.

3.2.2. Model assumptions

The TBR model incorporates the following assumptions:

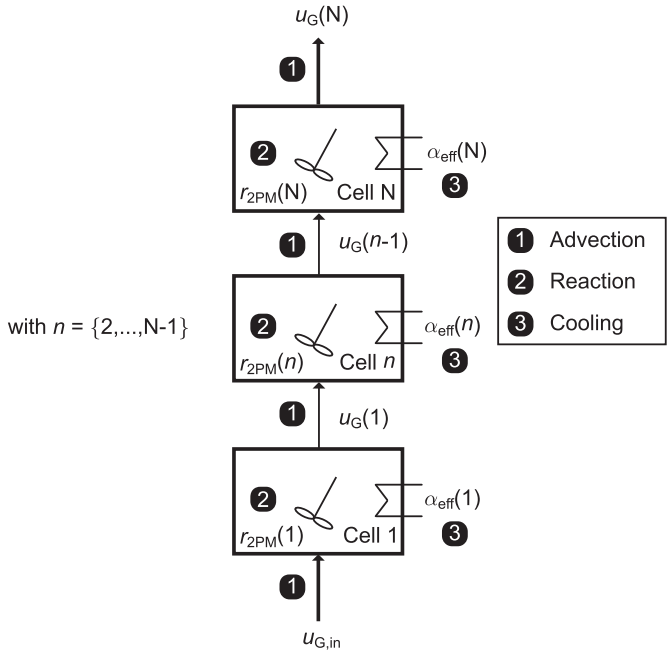

Fig. 5. Structure of the tube bundle reactor model, including the parameters influencing the mass and heat transfer phenomena.

1. Gas phase is assumed ideal, i.e. $c_{i,G}$ $p_i/(RT)$;
2. No distinction is made between concentration or temperature in the bulk gas phase and catalyst phase; only the intra particle mass transfer is taken into account with the catalyst efficiency η_{cat}, i.e. $c_{i,S}(z)$ $\eta_{cat}, c_{i,G}(z)$ and $T_G(z)$ $T_S(z)$ $T(z)$;
3. Plug flow is assumed, i.e. mass dispersion in the axial direction is neglected;
4. Thermal heat conduction, i.e. heat dispersion in the axial di rection is neglected;
5. Reactor wall is not taken into account for energy balance (accumulation term) and heat transfer.

Model assumptions are discussed in the supplementary materials.

3.2.3. Mole and energy balance

Using these assumptions, the mole and energy balances for the TBR can be written as follows.

Mole balance for the gas phase (Eq. (14)):

$$\underbrace{\varepsilon_{bed}, \frac{\partial c_G}{\partial t}}_{\text{Accumulation}} \quad \underbrace{\frac{\partial}{\partial z}(u_G, c_G)}_{\text{Advection}} + \underbrace{\sum_i \nu_i, \eta_{cat}, (1 \quad \varepsilon_{bed}), \rho_S, r_{2PM}}_{\text{Reaction}} \tag{14}$$

Mole balance for a gas species i in the gas phase (Eq. (15)):

$$\underbrace{\varepsilon_{bed}, \frac{\partial c_{i,G}}{\partial t}}_{\text{Accumulation}} \quad \underbrace{\frac{\partial}{\partial z}(u_G, c_{i,G})}_{\text{Advection}} + \underbrace{\nu_i, \eta_{cat}, (1 \quad \varepsilon_{bed}), \rho_S, r_{2PM}}_{\text{Reaction}} \tag{15}$$

Energy balance (Eq. (16)):

$$\underbrace{(\rho_G, c_{p,G}, \varepsilon_{bed} + \rho_S, c_{p,S}, (1 \quad \varepsilon_{bed})), \frac{\partial T}{\partial t}}_{\text{Accumulation}} \quad \underbrace{\frac{\partial}{\partial z}(\rho_G, c_{p,G}, u_G, T)}_{\text{Advection}}$$

$$\underbrace{+\eta_{cat}, (1 \quad \varepsilon_{bed}), \rho_S, r_{2PM}, (\quad Dh_r)}_{\text{Reaction heat}} \underbrace{\frac{4, \alpha_{eff}}{d_{tube}}, (T \quad T_{cool})}_{\text{Cooling}} \tag{16}$$

3.2.4. Reaction rate

The intrinsic reaction rate r_{2PM} was calculated using the kinetic rate equation based on the measurements shown in Ref. [94], while the catalyst efficiency was calculated through estimation of the Thiele modulus (see Eq. (27) and Eq. (28) in the Appendix).

3.2.5. Heat transfer

The effective heat transfer coefficient was calculated with Eq. (17):

$$\alpha_{\text{eff}} \quad \frac{1}{\frac{1}{\alpha_{\text{wall}}} + \frac{d_{\text{tube}}}{8 \cdot \lambda_{\text{r,eff}}}} \tag{17}$$

The wall heat transfer coefficient α_{wall} was calculated using a correlation developed by Martin and Nilles [95] for heat transfer in fixed bed reactors (see Appendix C.3). This correlation is valid for a Peclet number *Pe* between 1 and 10000 and $d_{\text{tube}}/d_{\text{P}}$ between 1.2 and 51. In this work, *Pe* lies between 100 and 400, while $d_{\text{tube}}/\ d_{\text{P}}$ is 6.6. Thus, the correlation of Martin and Nilles is valid for this TBR simulation. The heat transfer coefficient on the cooling side of the reactor was assumed to be high and not limiting. Furthermore, the cooling medium temperature was assumed to be constant due to a large cooling medium flow rate.

The effective radial heat conductivity $\lambda_{\text{r,eff}}$ of the bed material (solid and gas phases) was calculated with the so called α_{w} heat transfer model, assuming constant heat conductivity along the radial coordinates (see Appenidix C.3). More detailed information on this model can be found in Ref. [72].

3.2.6. Momentum balance

Along Eq. (14) to Eq. (16), the momentum balance expressed in Eq. (18) (Ergun equation [96]) had to be solved to account for the pressure drop along the fixed bed.

$$\frac{\partial p}{\partial z} \quad \frac{u_{\text{G}}}{d_{\text{P}}} \cdot \frac{1 \quad \varepsilon_{\text{bed}}}{\varepsilon_{\text{bed}}^3} \cdot \left(1.75 \cdot \rho_{\text{G}} \cdot u_{\text{G}} + 150 \cdot \frac{\mu_{\text{G}}}{d_{\text{P}}} \cdot (1 \quad \varepsilon_{\text{bed}})\right) \tag{18}$$

The decrease in superficial gas velocity along the reactor height due to chemical reaction was calculated by solving Eq. (14).

3.2.7. Numerical procedure

In the Matlab® ode15s solver, Eq. (14) to Eq. (16) were solved with the MOL, i.e. the PDE along the vertical axis were discretized, while the solver integrated the ODE along time. The reactor was discretized in cells with a height *dz* 0.005 m.

3.2.8. Reactor design strategy

A TBR design optimizing heat transfer was chosen: the pellet catalyst (d_{P} 0.003 m) is distributed over several tubes ($d_{\text{tube,in}}$ 0.02 m) reaching a packed bed porosity ε_{bed} of 0.4. The maximum inlet gas velocity in each tube $u_{\text{G,in}}$, was set to 1.0 m/s in order to mitigate pressure drop, leading to a number of tubes N_{tube} of 80. The maximum catalyst temperature allowed for continuous operation is 510 °C. The TBR was designed accordingly. The TBR boundary conditions as well as their justification are listed in Table 3.

In order to reach a CO_2 conversion of 0.9 and keep the maximum reactor temperature below 510 °C, two parameters could be varied: the reactor length L_{R} and the cooling medium temperature T_{cool}. First, these two parameters were guessed and the Matlab® solver was started. L_{R} and T_{cool} were then iteratively varied until the desired CO_2 conversion and maximum reactor temperature were achieved. This algorithm is illustrated in Fig. 33 in the supplementary materials.

Table 3
Tube bundle reactor boundary conditions.

Parameter	Value	Justification
T_{in}	T_{cool}	Reduction of reactor variables[a]
$d_{\text{tube,in}}$	2·10 ^{2} m	Optimal heat transfer
$u_{\text{G,in,max}}$	≤1 m/s	Pressure drop mitigation
N_{tube}	80	Derived from $u_{\text{G,in,max}}$ and $V_{\text{in,STP}}$
ε_{bed}	0.4	Reaction and heat transfer enhancement

[a] This corresponds to a reactor design where the cooling medium preheats the inlet gas flow. The influence of inlet gas temperature on the performance of the TBR is shown in Fig. 19 in the supplementary materials.

4. Results and discussion

Aim of this publication was to study the behavior of a SBCR and a TBR for transient PtG operations. Beforehand, reactor designs had to be determined using the boundary conditions given in Tables 2 and 3; these designs are presented in section 4.1. Once the reactor designs were established, the evolution of local reactor temperature as well as CO_2 conversion integrated along the vertical axis of each reactor were discussed for both reactors. Then, a sensitivity analysis was performed to assess the reliability of each reactor model. To conclude section 4.1, a reactor control strategy was defined for the different gas loads applied for transient PtG operation.

The results of transient PtG operation are presented in section 4.2. First, the effect of a gas load increase on methanation reactor performance was studied with dimensionless numbers. Once this effect was clarified, results of transient methanation reactor operation were discussed. Finally, solutions to improve the performance of both methanation reactors were proposed.

4.1. Determination of methanation reactor design

4.1.1. Slurry bubble column reactor design

Aim of the following study was to find the combination of $h_{\text{R}}/d_{\text{R}}$ and φ_{S} maximizing the reactor *GHSV*, i.e. the reactor performance, for a maximum volume flow rate of 900 m^3/h and a CO_2 conversion X_{CO_2} of 0.9. The results of this study are shown in Fig. 6. For $0 \leqslant \varphi_{\text{S}} \leqslant 0.12$, $h_{\text{R}}/d_{\text{R}}$ rapidly decreases from 55 to 8, while *GHSV* rapidly increases from 500 to 3500 1/h. For $0.12 \leq \varphi_{\text{S}} \leq 0.2$, $h_{\text{R}}/d_{\text{R}}$ decreases slowly, while *GHSV* increases slowly until an optimum is reached with $h_{\text{R}}/d_{\text{R}}$ 7.4 and *GHSV* 3918 1/h. A further increase in φ_{S} leads to a slow increase in $h_{\text{R}}/d_{\text{R}}$ and a decrease in *GHSV*.

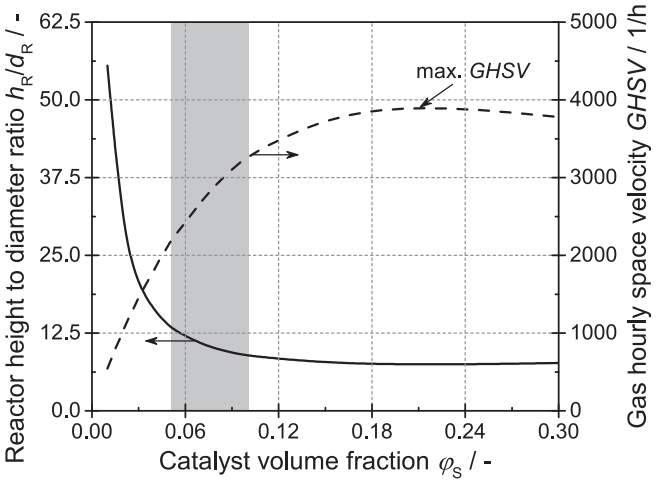

Fig. 6. Combinations of catalyst volume fraction, required reactor height-to-diameter ratio and gas hourly space velocity of the slurry bubble column reactor which allow a CO_2 conversion of 0.9 with a feed $H_2/CO_2/CH_4$ of 4/1/1 and a volume flow rate of 900 m^3/h ($\overline{T}_{\text{SL}}$ 320 °C, p_{out} 20 bar, $u_{\text{G,in}}$ 0.3 m/s). Grey-marked area corresponds to the range of catalyst volume fraction for an investment/operation cost optimization.

A SBCR is usually either limited by chemical reaction rate or by gas/liquid mass transfer [97,98]. Chemical reaction rate is enhanced by increasing catalyst volume fraction (see Eq. (9)), while gas/liquid mass transfer is decreased by increasing catalyst volume fraction [83]. The limiting reaction step can be identified in Fig. 6; for $\varphi_S \leq$ 0.2 the chemical reaction is the limiting reaction step, as an in crease in φ_S leads to higher *GHSV*. However, for $\varphi_S > 0.2$ an increase in φ_S no longer enhances *GHSV*; the SBCR is limited by gas/liquid mass transfer.

Furthermore, a grey area is pictured in Fig. 6 which corresponds to the range of φ_S for an investment/operation cost optimization: at $\varphi_S < 0.05$ the resulting SBCR is too large to be cost effective, while at $\varphi_S > 0.1$ an increase in catalyst volume fraction does not lead to a substantial decrease in reactor volume. The catalyst concentration of a commercial SBCR for three phase CO_2 methanation lies therefore in this range. Nevertheless, in this work both SBCR and TBR are compared using a reactor design maximizing *GHSV*, i.e. maximizing the specific reaction heat release which corresponds to the most challenging scenario in terms of heat management. As a consequence, a catalyst volume fraction of 0.2 corresponding to a h_R/d_R of 7.4 and a *GHSV* of 3918 1/h were used as SBCR design parameters for the following simulations. All SBCR design param eters are summarized in Table 4.

Based on this study, the evolution of local slurry temperature $T_{SL}(z)$ as well as CO_2 conversion $X_{CO_2}(z)$ integrated along the ver tical axis of the SBCR was calculated. The results are shown in Fig. 7.

From the bottom to the top of the SBCR, T_{SL} decreases from 323 to 317 °C. Hence, the SBCR can be considered as quasi isothermal. The evolution of T_{SL} is correlated to X_{CO_2} and the corresponding reaction heat release: 50% of the CO_2 conversion takes place in the first 30% of reactor volume (bottom), while only 10% of the CO_2 conversion takes place in the last 30% of reactor volume (top). Considering that cooling occurs in the slurry phase with constant specific heat transfer area and constant cooling medium tempera ture, T_{SL} is accordingly higher than 320 °C at the reactor bottom and lower than 320 °C at the reactor top.

To assess the reliability of the SBCR model, a sensitivity analysis was carried out on the most critical SBCR model parameters, i.e. the parameters controlling the effective reaction rate; the gas holdup ε_G, the gas/liquid mass transfer coefficient $k_L a_i$, and the intrinsic CO_2 methanation reaction rate r_{3PM}. The uncertainty of ε_G, $k_L a_i$ and r_{3PM} were taken from literature, [82,83,92]. These uncertainties were ±42%, ±36%, and ±10.6%, respectively. An extreme case sce nario was obtained by setting simultaneously the uncertainty of each parameter to its maximum or minimum value. The results of the sensitivity analysis are shown in Fig. 8.

Table 4
Slurry bubble column reactor design parameters to reach a CO_2 conversion of 0.9 for a feed $H_2/CO_2/CH_4$ of 4/1/1 with a volume flow rate of 900 m^3/h (STP).

Parameter	Value
$\overline{T}_{SL}$	320 °C
$T_{SL,max}$	350 °C
$T_{G,in}$	$\overline{T}_{SL}$
d_P	$75 \cdot 10^{-6}$ m
d_{hole}	$1 \cdot 10^{-4}$ m
a_{free}	$7.2 \cdot 10^{3}$
N_{hole}	83095
$u_{G,in,max}$	0.3 m/s
a_{cool}	10 m^2/m^3
d_R	0.34 m
φ_S	0.2
h_R	2.53 m
GHSV	3918 1/h

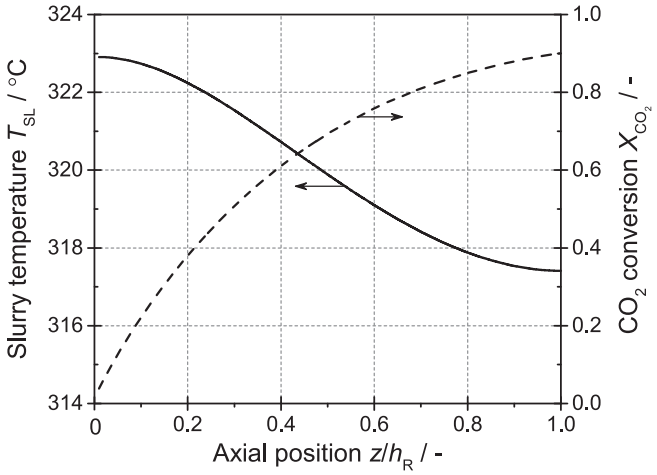

Fig. 7. Evolution of local slurry temperature and CO_2 conversion integrated along the axial direction of the slurry bubble column reactor for a feed $H_2/CO_2/CH_4$ of 4/1/1 (Reactor design parameters are summarized in Table 4, T_{cool} 269 °C).

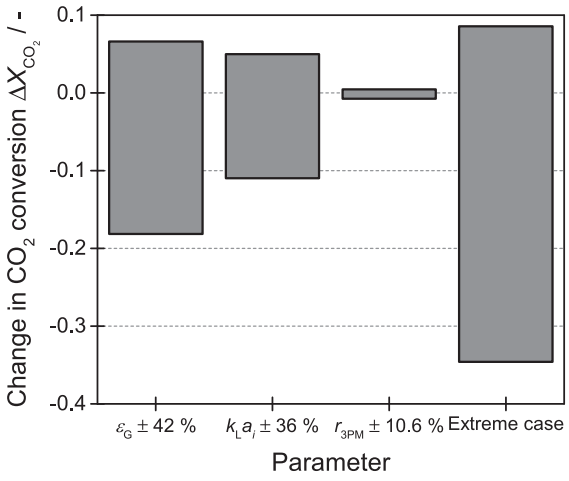

Fig. 8. Sensitivity analysis based on the uncertainties of gas holdup and gas/liquid mass transfer coefficient correlations as well as kinetic rate equation for the slurry bubble column reactor with a feed $H_2/CO_2/CH_4$ of 4/1/1 (Reactor design parameters are summarized in Table 4, reference X_{CO_2} 0.9).

The reaction rate is the least sensitive parameter, followed by $k_L a_i$ and ε_G. This order was expected, as the SBCR is mass transfer limited and not chemical reaction limited. As a consequence, a change in r_{CO_2} of ±10.6% has a small influence on X_{CO_2} (around ± 0.01). The gas/liquid mass transfer $k_L a_i$ has a much higher influence as it controls the reaction limiting step: a decrease in $k_L a_i$ of 36% results in a decrease in X_{CO_2} of ca. 0.11. The influence of ε_G on X_{CO_2} is even higher than the influence of $k_L a_i$. In the $k_L a_i$ correlation developed by Lemoine et al. [83] $k_L a_i$ is proportional to $\varepsilon_G^{1.21}$. As a consequence, an uncertainty in ε_G results in an even higher uncertainty in $k_L a_i$. Considering the extreme case scenario, the parameter uncertainties can lead to a deviation in X_{CO_2} of 0.35. This shows the current need for more accurate ε_G and $k_L a_i$ correlations.

However, if a reactor design with a volumetric catalyst con centration of 0.07 had been chosen, i.e. in the economical range (see Fig. 6), the results of a sensitivity analysis should be different. For this catalyst concentration, the reactor is limited by chemical re action and not by mass transfer. As a consequence, for φ_S 0.07 the

reactor should be much more sensitive to a change in r_{3PM}.

4.1.2. Tube bundle reactor design

Aim of the following study was to identify a combination of reactor length L_R and cooling medium temperature T_{cool} which maximizes *GHSV* for a maximum volume flow rate of 900 m^3/h and a CO_2 conversion X_{CO_2} of 0.9, while keeping T_{max} below 510 °C. The results of this study are shown in Fig. 9. For increasing T_{cool}, both T_{max} and *GHSV* increase. Furthermore, for 227 °C < T_{cool} < 245 °C, the increase in *T* and *GHSV* is higher. Increasing temperatures enhance chemical reaction rate. An increase in T_{cool} results in higher reactor temperatures which enhance the reaction rate and allow for higher *GHSV*.

The two grey areas marked in Fig. 9 (I and II) correspond to operating conditions which are not desired for the design of a TBR for CO_2 methanation. Area I is characterized by $\Delta T_{max}/\Delta T_{cool} > 5$: a small increase in T_{cool} results in a high change in T_{max}. It is critical to design a TBR in area I, considering that a change in cooling tem perature of less than 1 K may lead to change in reactor temperature between 5 and 25 K. As such the cooling medium temperature range 227 °C ≤ T_{cool} ≤ 245 °C is not desirable. Area II is charac terized by T_{max} > 510 °C, i.e. temperatures which favor thermal catalyst degradation according to the specifications of the catalyst supplier. Thus, conditions with T_{cool} higher than 252 °C are not acceptable. Higher cooling temperature could be chosen, if a cata lyst with higher temperature stability can be implemented.

Two ranges of cooling temperature can be used for the design of the TBR: T_{cool} < 227 °C, and 245 °C < T_{cool} < 252 °C. Choosing T_{cool} < 227 °C results in a TBR with low *GHSV* (<2500 1/h). The maximum possible *GHSV* of about 59,683 1/h is achieved at T_{cool} 251 °C and L_R 0.6 m. These parameters are in conse quence used as TBR design parameters for further simulations. All the TBR design parameters are summarized in Table 5.

Based on this study, the evolution of the local reactor temper ature $T_R(z)$ and CO_2 conversion $X_{CO_2}(z)$ integrated along the vertical axis of the TBR is shown in Fig. 10. Between 0 and 60% of the reactor volume, T_R rises slowly from 251 °C to 350 °C, which results in an increase in X_{CO_2} of only 0.35. Between 60 and 80% of the reactor volume, the increase in T_R is significant: ΔT_R 230 K. It results in a considerable increase in X_{CO_2} of 0.45. Between 80 and 100% of the

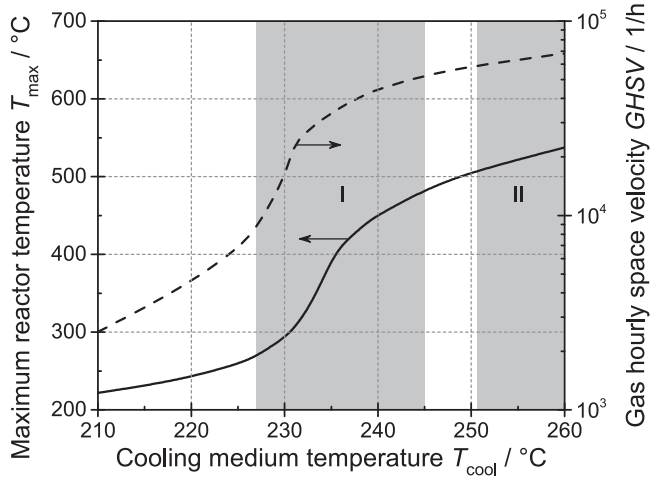

Fig. 9. Combinations of cooling medium temperature, maximum reactor temperature and gas hourly space velocity of the tube bundle reactor which allow for a CO_2 conversion of 0.9 with a feed $H_2/CO_2/CH_4$ of 4/1/1 and a volume flow rate of 900 m^3/h (p_{in} 20 bar, $u_{G,in}$ 0.97 m/s). Grey-marked areas correspond to non-acceptable operating conditions (I: high sensitivity to cooling, II: thermal catalyst degradation).

Table 5
Tube bundle reactor design parameters to reach a CO_2 conversion of 0.9 for a feed $H_2/CO_2/CH_4$ of 4/1/1 with a volume flow rate of 900 m^3/h (STP).

Parameter	Value
T_{in}	T_{cool}
$d_{tube,in}$	2·10 ^{2} m
$u_{G,in,max}$	0.97 m/s
N_{tube}	80
ε_{bed}	0.4
L_R	0.6 m
GHSV	59,683 1/h

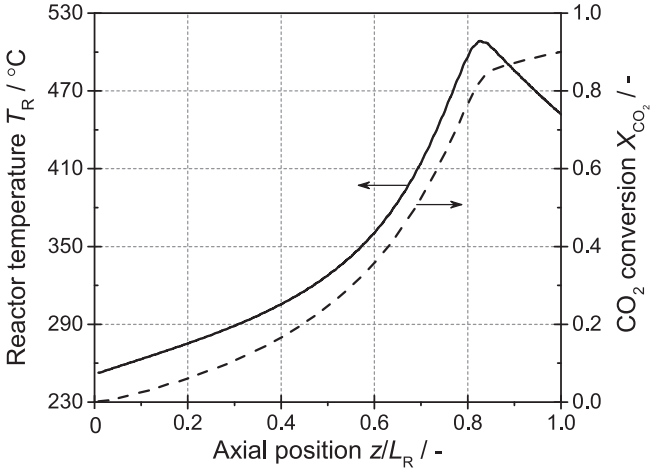

Fig. 10. Evolution of local reactor temperature and CO_2 conversion integrated along the axial direction of the tube bundle reactor for a feed $H_2/CO_2/CH_4$ of 4/1/1 (Reactor design parameters are summarized in Table 5, T_{cool} 251 °C).

reactor volume, T_R decreases while X_{CO_2} slowly rises from 0.8 to 0.9. Under these conditions, the chemical reaction rate slows down due to thermodynamic limitation.

A sensitivity analysis was carried out on the most critical pa rameters of the TBR model to assess the simulation reliability. These parameters control the reaction rate or the heat transfer: the tube wall heat transfer coefficient α_{wall}, the effective radial heat conductivity $\lambda_{r,eff}$, and the kinetic rate equation for CO_2 methana tion r_{2PM}.

The uncertainties of α_{wall} and r_{2PM} were taken from literature and are ±30% and ±10.6%, respectively. The uncertainty related to $\lambda_{r,eff}$ correlation could not be found in the literature (see Appendix C.3.3). Thus, the uncertainty of $\lambda_{r,eff}$ was set to ±30%. An extreme case scenario is obtained by setting simultaneously the uncertainty of each parameter to its maximum or minimum value. The results of this sensitivity analysis are shown in Fig. 11.

The uncertainties related to α_{wall} and $\lambda_{r,eff}$ have almost no in fluence on X_{CO_2}: a change of only ±0.01 is observed. However, the maximum reactor temperature T_{max} does change ca. ± 30 K. A rise in α_{wall} and $\lambda_{r,eff}$ increases the effective heat transfer coefficient. Hence, the reactor temperature decreases as well as the effective reaction rate and the gas superficial velocity. The decrease in u_G results in higher gas residence time, which compensates for the lower reaction rates and results in almost no change in X_{CO_2}. A decrease in r_{2PM} of 10.6% has a higher impact on the achievable X_{CO_2} with a change of ca. 0.1. The TBR simulated in this work is a polytropic reactor and is strongly affected by a change in r_{2PM} which impacts the evolution of temperature and gas concentra tions along the whole reactor length. An increase in r_{2PM} of +10.6%

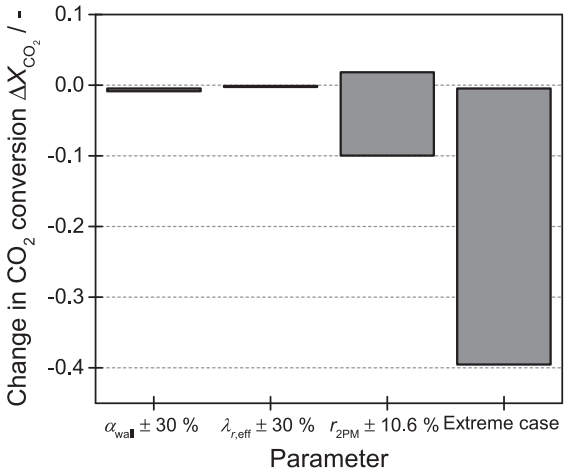

Fig. 11. Sensitivity analysis based on the uncertainties of heat transfer coefficient and radial heat conductivity correlations as well as kinetic rate equation for the methanation tube bundle reactor with a feed $H_2/CO_2/CH_4$ of 4/1/1 (Reactor design parameters are summarized in Table 5, reference X_{CO_2} 0.9).

has less impact on X_{CO_2} because X_{CO_2} is already high and the reaction is limited by thermodynamic equilibrium and not chemical reaction kinetics. Finally, considering an extreme case scenario, a simultaneous increase in α_{wall}, $\lambda_{r,eff}$ and r_{2PM} results in a significant decrease in X_{CO_2} of ca. 0.4. Under these conditions, the cooling rate is strongly enhanced, which mitigates the formation of a hot spot: a maximum reactor temperature of only 353 °C is reached. As a consequence lower reaction rates are achieved which decrease X_{CO_2}.

4.1.3. Reactor control strategy

For PtG applications, a methanation reactor must be able to adapt to a fluctuating H_2 volume flow rate, while maintaining a constant H_2/CO_2 ratio of 4. For a given gas volume flow rate, the cooling medium temperature must be adapted, so that the methanation reactor respects its boundary conditions ($X_{CO_2} \geq 0.9$, as well as all parameters given Tables 2 and 3). For transient operation, the previously designed SBCR and TBR should operate between 25 and 100% of the maximum gas load. The corresponding cooling medium temperatures derived from steady state simulations are summarized in Table 6.

Table 6 shows that X_{CO_2} decreases in both reactors for increasing gas load. However, the SBCR requires a reduced T_{cool} for increasing gas load, while the TBR needs increased T_{cool}; this behavior is explained in section 4.2.1. Furthermore, at 25% of the maximum gas load the TBR is characterized by $\Delta T_{max}/\Delta T_{cool} > 5$. As safe steady state operation cannot be guaranteed under this operating condition (see Fig. 9), transient TBR operation at gas loads below 50% is not considered.

To summarize, the SBCR is an almost isothermal reactor which is limited by gas/liquid mass transfer. On the other hand, the TBR is mostly limited by heat transfer. Contrary to the SBCR, the TBR is a polytropic reactor which offers higher reaction rates. Hence, much higher *GHSV* can be reached in a TBR (in this case, ca. 60,000 1/h) compared to a SBCR (*GHSV* 4000 1/h). For steady state operation, a TBR is to be preferred to a SBCR. However, a TBR may not be suited for transient operation, as it is very sensitive to a gas load variation, leading to significant changes in advective heat transfer and cooling rate.

4.2. Transient power to gas operation

4.2.1. Effect of gas load increase on methanation reactor performance

As preliminary for transient PtG operation, a study was carried out to understand the effect of gas load increase on the SBCR and the TBR performance via comparison of dimensionless numbers for mass and heat transfer. These dimensionless numbers are derived from the differential equations describing the mass and heat balance of the reactor (SBCR: Eqs. (9) and (10), TBR: Eqs. (15) and (16)). They compare axial dispersion, gas/liquid mass transfer, chemical reaction or convective heat transfer with advection. These dimensionless numbers are:

- $1/Pe'$, i.e. diffusive mass transfer vs. advective mass transfer;
- $1/Pe$, i.e. diffusive heat transfer vs. advective heat transfer;
- Sh/Pe', i.e. gas/liquid mass transfer vs. advective mass transfer;
- Da_I, i.e. reaction rate vs. advective mass transfer;
- Da_{III}, i.e. reaction heat release rate vs. advective heat transfer;
- St, i.e. convective heat transfer vs. advective heat transfer.

The results of this study are shown in Figs. 20–23 in the supplementary materials and are summarized in Tables 7 and 8.

Table 7 shows that a gas load increase in a SBCR leads to a rise in axial dispersion and gas/liquid mass transfer, which results in lower axial gradients of gas concentrations and temperature, and higher gas concentrations in the liquid phase, respectively. Due to the higher gas concentrations in the liquid phase the overall reaction rate increases, which also results in higher reaction heat release rate. The convective heat transfer of a SBCR is insensitive to an increase in gas load for gas superficial velocity higher than 0.1 m/s. As a consequence, the heat transfer coefficient of the SBCR is unchanged. These phenomena result in a small increase in SBCR temperature and small decrease in CO_2 conversion X_{CO_2}.

Table 8 shows that a gas load increase in a TBR results also in lower gas residence time. Besides, it displaces the reactor hot spot to higher axial coordinates. The overall reaction rate is increased by the higher gas concentrations, which results in higher reaction heat release rate. However, the convective heat transfer is also largely increased, which results in much higher cooling rate. The resulting cooling rate is higher than the reaction heat release rate. Consequently, the temperature of the TBR as well as CO_2 conversion decrease significantly.

Table 6
Reactor cooling medium temperature for different gas loads. Reactor design parameters are summarized in Tables 4 and 5

	SBCR		TBR	
Load/%	T_{cool} / °C	X_{CO_2} /-	T_{cool} / °C	X_{CO_2} /-
25	300	0.975	*206*	*0.968*
50	289	0.964	226	0.942
75	278	0.933	240	0.92
100	269	0.9	251	0.9

Table 7
Effect of gas load increase on SBCR performance for a constant cooling medium temperature.

Phenomena	Change	Effect
Advection	↗↗↗	Lower gas residence time
Axial dispersion	↗	Lower axial c_i and T gradient
G/L mass transfer	↗↗	Higher $c_{i,L}$
Chemical reaction	↗↗	Higher reaction rate and heat release rate
Convective heat transfer		Constant heat transfer coefficient

Table 8
Effect of gas load increase on TBR performance for a constant cooling medium temperature.

Phenomena	Change	Effect
Advection	↗↗↗	Lower gas residence time, and hot spot translation to higher z
Chemical reaction	↗↗	Higher reaction rate and heat release rate
Convective heat transfer	↗↗↗	Higher heat transfer coefficient

4.2.2. Transient slurry bubble column reactor

The evolution of the mean slurry temperature $\overline{T}_{SL}$ over time is shown in Fig. 12 for a gas load step increase from 75 to 100% of the maximum reactor gas load.

The new load is reached after 1 s. Following this change $\overline{T}_{SL}$ increases from 320 to 330 $^{+}$C; a stationary state is reached after ca. 600 s. Due to the high heat transfer coefficient (ca. 2300 W/(m^2,K) and the high heat capacity of the slurry phase (ca. 1600 kJ/(m^3,K)), a minor increase in $\overline{T}_{SL}$ of only 10 K takes place, while X_{CO_2} de creases from 0.933 to 0.904. Due to the increase in gas velocity, the gas residence time is reduced, while the increased slurry temper ature leads to higher reaction rates. Altogether, the higher reaction rates do not compensate for the shorter residence time, which re sults in a lower X_{CO_2}. However, at any time $X_{CO_2} > 0.9$ and $T_{SL} < 350$ $^{+}$C is given. Hence, all SBCR boundary conditions are respected: the SBCR design is adequate for this transient operation.

The evolution of the mean slurry temperature $\overline{T}_{SL}$ over time after a gas load decrease from 100 to 75% is shown in Fig. 24 in the supplementary materials. Similar results are obtained: the SBCR design is suitable for this transient methanation operation. This statement applies also for the other gas load changes shown in Figs. 25–28 in the supplementary materials. Even for the large gas load change of ±50%, the SBCR boundary conditions are respected. As such the SBCR designed in this work is a suitable CO_2 metha nation reactor for the suggested transient PtG operating conditions.

4.2.3. Transient tube bundle reactor

The evolution of the maximum reactor temperature T_{max} over time is shown in Fig. 13 for a gas load increase from 75 to 100% of the maximum reactor gas load. The new load is reached in 1 s. Following this change, T_{max} rises from 510 to 579 $^{+}$C within 7 s and then decreases to 351 $^{+}$C within the next 11 s. After 18 s the TBR has reached the new steady state: the TBR response is 33 times faster than the SBCR response.

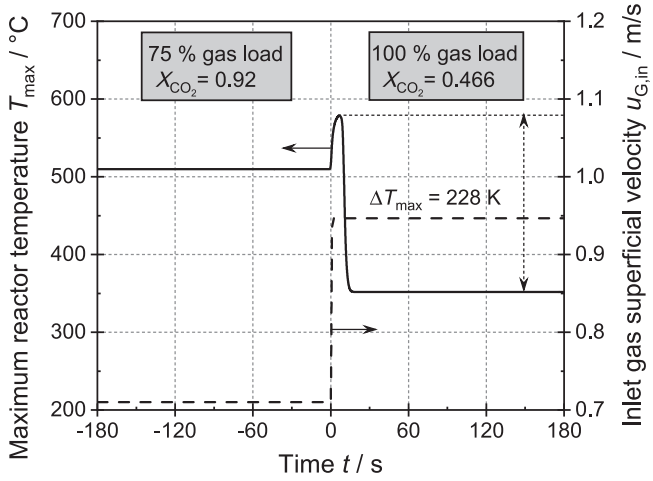

Fig. 13. Maximum reactor temperature of the tube bundle reactor as function of time after a gas load step change from 75 to 100% for a feed $H_2/CO_2/CH_4$ of 4/1/1 (Reactor design parameters are summarized in Table 5, T_{cool} 240 $^{+}$C).

The evolution of T_{max} over time is related to the combination of mass transfer and heat transfer phenomena, which are illustrated in Fig. 14. An increase in gas inlet velocity enhances the advective mass transfer: a higher amount of educts can react in the reactor which results in an increase in reaction heat release rate. As a consequence T_{max} increases. Following the gas velocity increase, advective heat transfer and cooling rate are also increased. The increased cooling rate results in lower reactor temperature, while the increased advective heat transfer shifts the reactor hot spot to the reactor outlet. Hence, the hot spot progressively disappears from the reactor and T_{max} decreases.

Fig. 14 shows also that X_{CO_2} decreases from 0.92 to 0.466

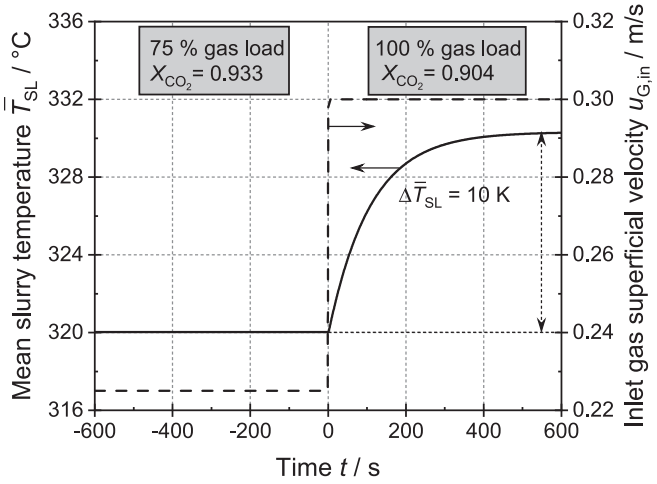

Fig. 12. Slurry temperature as function of time after a gas load step change from 75 to 100% for a feed $H_2/CO_2/CH_4$ of 4/1/1 (Reactor design parameters are summarized in Table 4, T_{cool} 278 $^{+}$C).

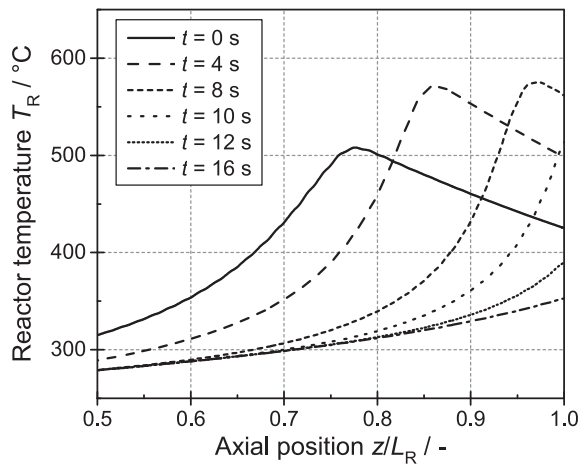

Fig. 14. Evolution of the reactor temperature along the axial direction of the tube bundle reactor after a gas velocity step change from 0.71 to 0.95 m/s (p_{in} 20 bar, L_R 0.6 m, T_{cool} 240 $^{+}$C).

comparing the two stationary states. The lower X_{CO_2} is related to the lower reactor temperature as well as the decreased gas resi dence time. The TBR response to a gas load change is not satisfying the design requirements. First, the catalyst reaches a temperature higher than the maximum of 510 °C. Then, the catalyst undergoes a high temperature change within a short period of time, which may result in mechanical stress leading to catalyst crushing and deac tivation. Finally, the outlet gas quality ($X_{CO_2} < 0.9$) is not satisfying the design requirements.

The evolution of the maximum reactor temperature T_{max} over time after a gas load decrease from 100 to 75% is shown in Fig. 30 in the supplementary materials. Again, the transient TBR response does not satisfy the design requirements. Although X_{CO_2} fulfills the required gas quality, T_{max} is above the maximum allowed catalyst temperature of 510 °C. Besides, the catalyst undergoes a temper ature change of 84 K within 15 s which may result in catalyst crushing and deactivation.

The other gas load variations show similar results (see Figs. 29–31 in the supplementary materials). Altogether the TBR design suggested in this work is not suitable for transient PtG operation. Solutions to overcome this issue are suggested in the following section.

4.3. Reactor improvement considerations

Dimensionless numbers are useful to characterize and under stand the interaction between mass transfer, heat transfer, and chemical reaction involved in reaction engineering. In this work, the Damkohler numbers II and III as well as the Stanton number are of special interest to understand the process involved in steady state and transient operations of a SBCR and a TBR for CO_2 methanation.

The Damkohler number II, Da_{II}, compares chemical reaction rate with mass transfer phenomena as shown in Eq. (19). Details related to the calculation of volumetric mass transfer coefficient $k_G a_{CO_2}$ and $k_L a_{CO_2}$ are given in the Appendix.

$$Da_{II} \quad \frac{\varphi_S \cdot \rho_S \cdot r_{CO_2}}{k_j a_{CO_2} \cdot c_{CO_2,G}} \tag{19}$$

The evolution of Da_{II} with increasing gas load is shown in Fig. 15 for both SBCR and TBR. $Da_{II,SBCR} > 1$, while $Da_{II,TBR} \ll 1$ over the whole range of gas load, i.e. the SBCR is moderately limited by gas/liquid mass transfer while the inter particle mass transfer is not limiting the TBR. To improve the efficiency of the SBCR, efforts should be made to enhance the gas/liquid mass transfer e.g. by increasing the specific gas/liquid interfacial area [97,98].

The transient Stanton number St' compares cooling rate with reactor heat accumulation as shown in Eq. (20). In Eq. (20), $\Delta T_R/\Delta t$ is set for both reactors to 40 K/h which corresponds to the maximum catalyst heating rate recommended by the catalyst supplier. However, as the reactors are compared with each other, the value of $\Delta T_R/\Delta t$ is not relevant.

$$St' \quad \frac{\alpha_{eff} \cdot a_{cool} \cdot (T_R \quad T_{cool})}{\rho \cdot c_p \cdot \frac{\Delta T_R}{\Delta t}} \tag{20}$$

The evolution of St' with increasing gas load is shown in Fig. 17. For both reactors, $St' >> 1$: heat accumulation is sensitive to a change in cooling rate. However, St'_{TBR} is 15–53 times higher than St'_{SBCR}. This explains the reactor response time shown in Figs. 12 and 13. As St'_{TBR} is high, the TBR reaches steady state after ca. 20 s, while the SBCR requires ca. 600 s to reach steady state.

Finally, the transient Damkohler number III Da'_{III} compares heat release rate from reaction with heat accumulation as shown in Eq. (21).

$$Da'_{III} \quad \frac{\phi_S \cdot \rho_S \cdot r_{CO_2} \cdot |\Delta h_r|}{\rho \cdot c_p \cdot \frac{\Delta T_R}{\Delta t}} \tag{21}$$

The evolution of Da'_{III} with increasing gas load is shown in Fig. 16 for both reactors. In both cases is $Da'_{III} >> 1$: the heat accumulation is sensitive to a change in reaction heat release rate. Nevertheless, $Da'_{III,TBR}$ is ca. 45 times higher than $Da'_{III,SBCR}$. Combined with St'_{TBR}, $Da'_{III,TBR}$ can explain the poor transient behavior of this TBR: this reactor is very sensitive to a change in reaction heat release rate and cooling rate, which results in significant variations in reactor temperature during transient operation. On the contrary, St'_{SBCR} and $Da'_{III,SBCR}$ are much lower due to the high heat capacity of the slurry phase: the SBCR is much less sensitive to change in reaction heat release rate or cooling rate and can successfully be operated under transient operating conditions.

Options to improve the transient behavior of the TBR are to reduce the catalyst volume fraction φ_S, to use a catalyst showing a lower methanation activity or to mix the catalyst with high heat capacity inert material in order to decrease Da'_{III}. However, this will

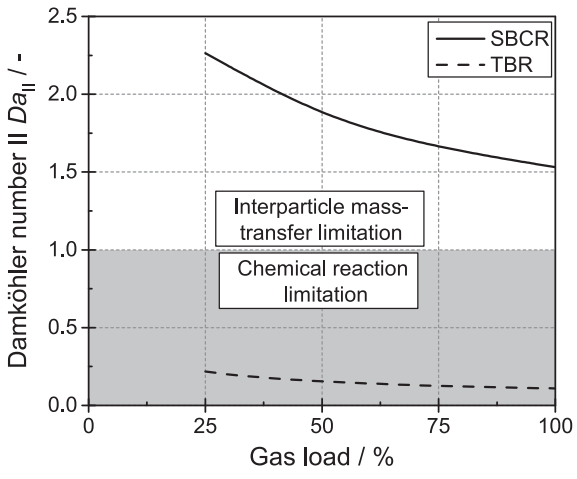

Fig. 15. Influence of gas load on Damkohler number II of the slurry bubble column reactor and the tube bundle reactor for a gas atmosphere $H_2/CO_2/CH_4$ of 4/1/1 (p_R 20 bar; φ_S 0.2, T_{SBCR} 320 °C; T_{STFR} 350 °C).

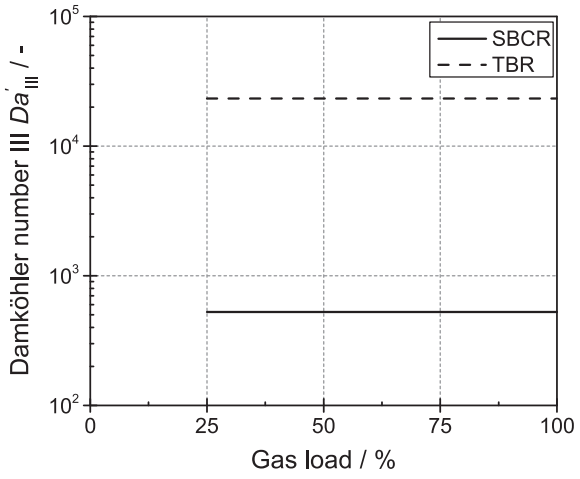

Fig. 16. Influence of gas load on transient Damkohler number III of the slurry bubble column reactor and the tube bundle reactor for a gas atmosphere $H_2/CO_2/CH_4$ of 4/1/1 (p_R 20 bar, $\Delta T_R/\Delta t$ 40 K/h; φ_S 0.2, T_{SBCR} 320 °C; T_{STFR} 350 °C.

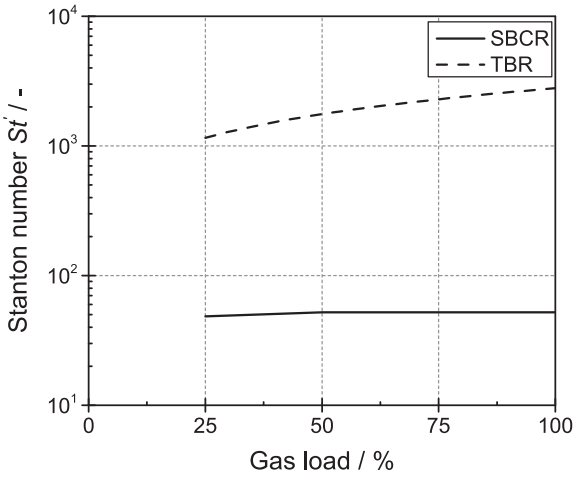

Fig. 17. Influence of gas load on transient Stanton number of the slurry bubble column reactor and the tube bundle reactor for a gas atmosphere $H_2/CO_2/CH_4$ of 4/1/1 (p_R 20 bar, $\Delta T_R/\Delta t$ 40 K/h; ϕ_S 0.2, T_{SBCR} 320 °C, $T_{cool,SBCR}$ 270 °C; T_{STFR} 350 °C, $T_{cool,STFR}$ 250 °C).

reduce the reactor *GHSV*.

5. Summary

In this publication, a slurry bubble column reactor (SBCR) and a state of the art tube bundle reactor (TBR) were modeled for cata lytic CO_2 methanation as part of a Power to Gas (PtG) process chain. The performances of the TBR and the SBCR were compared for steady state and transient Power to Gas (PtG) operations. Transient PtG conditions were modeled using gas load step changes between 25 and 100% of the reactor maximum capacities. The duration of the step was set to 1 s.

For steady state operation the TBR offers much higher gas hourly space velocities (*GHSV*) as compared to the SBCR. for tran sient PtG operation, the STFR undergoes significant temperature changes within a short time resulting in undesired outlet gas qualities violating product gas specifications. On the contrary, the SBCR temperature is kept under control and changes slowly upon transient operating conditions, while the outlet gas composition sticks to the gas quality requirements.

Finally, measures to improve the efficiency of both reactors were proposed considering dimensionless numbers. The *GHSV* of the SBCR can be enhanced by increasing the specific interfacial area controlling gas/liquid mass transfer, while the transient behavior of the STFR can be enhanced by reducing the catalyst concentration/ activity or by mixing the catalyst with high heat capacity inert material in detriment of the *GHSV*.

In terms of further work, the thermal integration of the SBCR within a PtG facility will be investigated under transient operating conditions. Especially, the transient behavior of heat exchangers will be taken into account for the simulation of the whole process chain. Finally, after providing a model for the description of a methanation plant under transient modes of operation, the inte gration of the PtG facility within a power and gas grid network will be undertaken as part of ongoing cooperation projects.

Declaration of competing interest

The authors declare that they have no known competing financial interests or personal relationships that could have appeared to influence the work reported in this paper.

Acknowledgements

This work was supported by Bundesministerium für Wirtschaft und Energie, Germany under the scope of RegEnKibo project (Grant number 03ET7542F).

Notation

Symbols (Latin)

Symbol	Description	Unit
a_j	volumetric surface area	1/m
A	surface	m^2
A_R	reactor cross sectional area	m^2
c_i	concentration	mol/m^3
c_i^*	concentration at gas/liquid equilibrium	mol/m^3
c_p	specific heat capacity at constant pressure	J/(kg·K)
d	diameter	m
$D_{i,j}$	diffusion coefficient	m^2/s
GHSV	gas hourly space velocity	1/h
h_R	reactor height	m
$H_{i,cc}$	dimensionless Henry law's constant	
H_2/CO_2	ratio between H_2 and CO_2 molar fraction	
Δh_r^θ	specific reaction enthalpy at standard conditions	J/mol
$k_j a_i$	volumetric mass-transfer coefficient	1/s
L	length	m
m	mass	kg
M	molecular mass	kg/mol
n	amount of substance	mol
N	number	
p	absolute pressure	bar
p_i	partial pressure	bar
p_0	absolute pressure at standard conditions	bar
r	radius	m
r_i	catalyst mass-specific reaction rate	mol/(kg·s)
R	universal gas constant	J/(mol·K)
t	time	s
T	absolute temperature	K or °C
$\overline{T}_{SL}$	mean slurry temperature	K or °C
u	superficial velocity	m/s
v	molar volume	m^3/mol
V	volume	m^3
$\dot{V}$	volume flow	m^3/s
w_j	mass fraction	
x,y,z	space coordinates	m
X_{CO_2}	CO_2 conversion	
y_i	gas molar fraction	

Symbols (Greek)

Symbol	Description	Unit
α	heat transfer coefficient	$W/(m^2·K)$
Δv_i	diffusion volume	
η_{cat}	catalyst efficiency	
λ	thermal conductivity	W/(m·K)
ε	porosity or void fraction	
μ	dynamic viscosity	Pa·s
ν_i	stoichiometric coefficient	
ρ	density	kg/m^3
σ	surface tension	N/m
φ_S	volumetric solid fraction	

Dimensionless numbers

Symbol	Description	Definition	Meaning
Da_{I}	Damkohler number I	$\frac{\rho_{\mathrm{P}} \cdot r_i \cdot L}{u \cdot c_i}$	$\frac{\text{Reaction rate}}{\text{Advective mass transfer}}$
Da_{II}	Damkohler number II	$\frac{\rho_{\mathrm{P}} \cdot r_i}{k_j a_i \cdot c_i}$ or $\frac{\rho_{\mathrm{P}} \cdot r \cdot L^2}{D_{i,\mathrm{eff}} \cdot c_i}$	$\frac{\text{Reaction rate}}{\text{Mass tranfer}}$
Da_{III}	Damkohler number III (steady state)	$\frac{\rho_{\mathrm{P}} \cdot r_i \cdot \lvert\Delta h_{\mathrm{r}}\rvert \cdot L}{\rho \cdot c_p \cdot u \cdot T}$	$\frac{\text{Reaction heat release rate}}{\text{Advective heat tranfer}}$
Nu	Nusselt number	$\frac{\alpha \cdot L}{\lambda}$	$\frac{\text{Convective heat transfer}}{\text{Conductive heat transfer}}$
Pe	Peclet number (heat)	$\frac{\rho \cdot c_p \cdot u \cdot L}{\lambda}$ $Re \cdot Pr$	$\frac{\text{Advective heat transfer}}{\text{Conductive heat transfer}}$
Pe'	Peclet number (mass)	$\frac{u \cdot L}{D_{i,j}}$ $Re \cdot Sc$	$\frac{\text{Advective mass transfer}}{\text{Diffusive mass transfer}}$
Re	Reynolds number	$\frac{\rho \cdot u \cdot L}{\mu}$	$\frac{\text{Inertia force}}{\text{Viscous force}}$
Sc	Schmidt number	$\frac{\mu}{D_{i,j} \cdot \rho}$	$\frac{\text{Diffusive momentum transfer}}{\text{Diffusive mass transfer}}$
Sh	Sherwood number	$\frac{k_{i,j} \cdot L}{D_{i,j}}$	$\frac{\text{Convective mass transfer}}{\text{Diffusive mass transfer}}$
St	Stanton number (steady state)	$\frac{\alpha}{\rho \cdot c_p \cdot u}$ $\frac{Nu}{Re \cdot Pr}$	$\frac{\text{Convective heat transfer}}{\text{Advective heat transfer}}$
Φ	Thiele modulus	$\frac{d_{\mathrm{P}}}{2} \cdot \sqrt{\frac{r_i \cdot \rho_{\mathrm{P}}}{D_{i,\mathrm{eff}} \cdot c_i}}$	$\frac{\text{Reaction rate}}{\text{Diffusive mass transfer}}$

Abbreviations

Symbol	Description
ADM	axial dispersion model
CAPEX	capital expenditure
CFD	computational fluid dynamics
CNG	compressed natural gas
CSTR	continuous stirred-tank reactor
DBT	dibenzyltoluene
EU	European Union
FTS	Fischer-Tropsch synthesis
LNG	liquefied natural gas
ODE	ordinary differential equation
PDE	partial differential equation
PEM	polymer electrolyte membrane
PFR	plug flow reactor
PtG	Power-to-Gas
SBCR	slurry bubble column reactor
SNG	synthetic natural gas
STP	standard Temperature and Pressure
(T 273.15 K, p 1.01315 bar)	
TBR	tube bundle reactor
3PM	three-phase methanation

Indices

Symbol	Description
ax	axial
bed	bed of catalyst
B	bubble
cat	catalyst
cool	cooling

(*continued on next page*)

(*continued*)

Symbol	Description
eff	effective
G	gas
hole	hole
i	index for gas species
in	inlet
j	index for phase
Kn	Knudsen
large	large bubbles
L	liquid
m	mass
max	maximum value
molecule	molecule
out	outlet
pore	pore
P	catalyst particle
r	reaction
R	reactor
small	small bubbles
S	solid
SL	slurry
*	phase equilibrium

Appendix

A Mass transfer in and around catalyst particles

The mass transfer coefficient between gas phase (bulk) and the catalyst particle can be estimated with Eqs. (22) and (23) [101]:

$$k_{\mathrm{G}} \quad \frac{Sh \cdot D_{12}}{d_{\mathrm{P}}} \tag{22}$$

$$Sh \quad \frac{1.15}{\sqrt{\varepsilon_P}} \cdot Re_0^{0.5} \cdot Sc^{1/3} \tag{23}$$

A.1 Effective pore diffusion coefficient in a catalyst particle, $\boldsymbol{D_{i,eff}}$

The effective pore diffusion coefficient can be calculated using Eq. (24), in which ε_P is the catalyst porosity estimated to be 0.4:

$$D_{i,eff} \quad D_{pore} \cdot \varepsilon_P^{1.5} \tag{24}$$

Assuming one cylindrical pore, the effective pore diffusion co efficient depends on the Knudsen diffusion and the molecular diffusion (see sections 11.1.5 and 11.2.5). This is represented in Eq. (25).

$$\frac{1}{D_{pore}} \quad \frac{1}{D_{12}} + \frac{1}{D_{Kn}} \tag{25}$$

The Knudsen diffusion for mesopores can be calculated with Eq. (26) (units are SI).

$$D_{Kn} \quad 9.7 \cdot r_{pore} \cdot \sqrt{\frac{T}{M_G}} \tag{26}$$

where T is the temperature in K and M_G is the molar mass in g/mol. In this work, the molar mass of CO_2 is used as it results in conser vative diffusion constant.

The average r_{pore} derived from BET experiments is $5 \cdot 10^{-9}$ m.

A.2 Catalyst efficiency, $\boldsymbol{\eta_{cat}}$

The catalyst efficiency can be calculated using Eq. (27) [75]:

$$\eta_{cat} \quad \frac{3}{\Phi} \cdot \left(\frac{1}{\tanh\Phi} \quad \frac{1}{\Phi} \right) \tag{27}$$

Φ is the Thiele modulus defined with Eq. (28) [75].

$$\Phi \quad \frac{d_P}{2} \cdot \sqrt{\frac{r_i \cdot \rho_P}{c_i \cdot D_{i,eff}}} \tag{28}$$

B Criteria for estimation of absence of mass and heat transfer limitation

The reaction rate of heterogeneous catalytic reaction can be limited by the chemical reaction itself or by mass and heat transfer. To identify the limiting reaction process, different criteria have been developed to estimate if the effective reaction rate $r_{i,eff}$ is controlled by mass and heat transfer [107]. The following criteria are valid for a reaction order of 1.

First of all the Weisz Prater criterium has to be fulfilled to assure the absence of intraparticle mass transfer limitations [102].

$$\frac{r_{i,eff} \cdot \rho_p \cdot d_p^2}{4 c_i \cdot D_{i,eff}} < 1. \tag{29}$$

Then, external mass transfer can be neglected if the Mears criterium is valid [73]:

$$\frac{r_{i,eff} \cdot \rho_p \cdot d_p}{c_i \cdot k_G} < 0.3. \tag{30}$$

The absence of heat transfer limitations inside the catalyst can be assumed when the Anderson criterium is fulfilled [74]:

$$\frac{r_{i,eff} \cdot |\Delta h_r| \cdot \rho_p \cdot d_p^2}{4 \lambda_{eff} \cdot T} < \frac{RT}{E_A}. \tag{31}$$

Finally, external heat transfer around the catalyst particle can be neglected when the second Mears criterium is valid [73]:

$$\frac{r_{i,eff} \cdot |\Delta h_r| \cdot \rho_p \cdot d_p}{\alpha_{eff} \cdot T} < \frac{0.3RT}{E_A}. \tag{32}$$

C Calculation of physical properties

C.1 Gas properties

C.1.1 Gas density, $\boldsymbol{\rho_G}$. The density of the gas mixture in kg/m^3 is calculated with the ideal gas law, see Eq. (33).

$$\rho_G \quad \frac{p \cdot M_G}{R \cdot T} \tag{33}$$

with

$$M_G \quad \sum_i y_i \cdot M_i \tag{34}$$

C.1.2 Dynamic viscosity, $\boldsymbol{\mu_G}$. The dynamic viscosity of a gaseous component in Pa·s is calculated with the following Equation (35) [103]:

$$\mu_{i,G} \quad A + B \cdot T + C \cdot T^2 + D \cdot T^3 + E \cdot T^4 \tag{35}$$

For the calculation of the viscosity of a gaseous mixture, the following formula is applied (Eq. (36)):

$$\mu_G \quad \sum y_i \cdot \mu_{i,G} \tag{36}$$

C.1.3 Specific heat capacity, $c_{p,G}$. The specific heat capacity of a gas mixture in J/kg is estimated using Eq. (37).

$$c_{p,G} \quad \frac{\sum_i y_i \cdot M_i \cdot c_{p,i}}{\sum_i y_i \cdot M_i} \tag{37}$$

The specific heat capacity of each gas component $c_{p,i}$ is calcu lated according to Equation (38). This correlation is taken from Ref. [104].

$$c_{p,i} \quad A + B \cdot T + C \cdot T^2 + D \cdot T^3 + \frac{E}{T^2} \tag{38}$$

C.1.4 Thermal conductivity, $\boldsymbol{\lambda_G}$. The thermal conductivity in W/(m·K) of a gas mixture is calculated as following (Eq. (39)):

$$\lambda_G \quad \sum_i y_i \cdot \lambda_i \tag{39}$$

The thermal conductivity of each gaseous component in W/m/K is estimated using Eq. (40) [103].

$$\lambda_i \quad A + B \cdot T + C \cdot T^2 + D \cdot T^3 + E \cdot T^4 \tag{40}$$

C.1.5 Binary molecular diffusion coefficient, $\boldsymbol{D}_{12}$. The binary diffusion coefficient in cm^2/s can be estimated with Eq. (41) from Ref. [104] Da 27:

$$D_{12} \quad \frac{0.00143 \cdot T^{1.75}\left(\left(M_1\right)^{-1} + \left(M_2\right)^{-1}\right)^{1/2}}{p\sqrt{2}\left(\left(\Delta_{v1}\right)^{1/3} + \left(\Delta_{v2}\right)^{1/3}\right)^2} \tag{41}$$

Δ_{vi} is the diffusion volume. For H_2 Δ_{vi} is 6.12 and 26.9 for CO_2 [104].

C.2 Slurry properties

C.2.1 Slurry density, $\boldsymbol{\rho_{SL}}$. Slurry density can be calculated with Eq. (42):

$$\rho_{SL} \quad \rho_L \cdot (1 \quad \varphi_S) + \rho_P \cdot \varphi_S \tag{42}$$

C.2.2 Slurry dynamic viscosity, $\boldsymbol{\mu_{SL}}$. Slurry viscosity can be calculated with Eq. (43) [105]:

$$\mu_{SL} \quad \mu_L \cdot (1 + 4.5 \cdot \varphi_S) \tag{43}$$

C.2.3 Slurry heat capacity, $\boldsymbol{c_{p,SL}}$. Slurry heat capacity can be calcu lated with Eq. (44) [93]:

$$c_{p,SL} \quad c_{p,L} \cdot (1 \quad w_S) + c_{p,S} \cdot w_S \tag{44}$$

C.2.4 Slurry heat conductivity, $\boldsymbol{\lambda_{SL}}$. Slurry heat conductivity can be calculated with Eq. (45) [93]:

$$\lambda_{SL} \quad \lambda_L \frac{2\lambda_L + \lambda_S \quad 2\varphi_S \cdot (\lambda_L \quad \lambda_S)}{2\lambda_L + \lambda_S + \varphi_S \cdot (\lambda_L \quad \lambda_S)} \tag{45}$$

C.2.5 Gas diffusion coefficient in liquid phase, $\boldsymbol{D_{i,L}}$. The gas diffusion coefficient in liquid phase $D_{i,L}$ can be estimated with Eq. (46) [106] (see publication for units):

$$D_{i,L} \quad \frac{7.4 \cdot 10^{-8} \cdot T \cdot M_L^{0.5}}{\mu_L \cdot V_{i,\text{molecule}}^{0.6}} \tag{46}$$

$V_{i,\text{molecule}}$ is the molecule volume. For CO_2, this volume is $34\ cm^3/(g \cdot mol)$ [106].

C.3 Fixed bed properties

C.3.1 Thermal conductivity of the catalyst bed, $\boldsymbol{\lambda_{bed}}$. The thermal conductivity of the catalyst bed λ_{bed} is calculated using the cor relation proposed by Tsotsas [72] (see Eq. (47)–(51)).

$$\lambda_{bed} \quad \lambda_G \cdot \left(1 \quad \sqrt{1} \quad \varepsilon_{bed} + \sqrt{1} \quad \varepsilon_{bed} \cdot k_c\right) \tag{47}$$

with

$$k_C \quad \frac{2}{N} \cdot \left(\frac{B}{N^2} \cdot \frac{k_P \quad 1}{k_P} \cdot ln\frac{k_P}{B} \quad \frac{B+1}{2} \quad \frac{B \quad 1}{N}\right) \tag{48}$$

and

$$N \quad 1 \quad \frac{B}{k_P} \tag{49}$$

with B calculated for catalyst particles assuming spheres.

$$B \quad 1.25 \cdot \left(\frac{1 \quad \varepsilon_{bed}}{\varepsilon_{bed}}\right)^{10/9} \tag{50}$$

with

$$k_P \quad \frac{\lambda_P}{\lambda_G} \tag{51}$$

C.3.2 Effective radial thermal conductivity of the catalyst bed, $\boldsymbol{\lambda_{eff,r}}$. The effective radial thermal conductivity of the catalyst bed is calculated according to Tsotsas [72] (see Eq. (52)).

$$\lambda_{eff,r} \quad \lambda_{bed} + \frac{Pe \cdot \lambda_G}{8} \tag{52}$$

with *Pe* the Peclet number defined with Eq. (53):

$$Pe \quad \frac{u_G \cdot \rho_G \cdot c_{p,G} \cdot d_P}{\lambda_G} \tag{53}$$

C.3.3 Heat transfer coefficient at the internal reactor wall, $\boldsymbol{\alpha_{wall}}$. The heat transfer coefficient in a fixed bed reactor α_{wall} is calcu lated using the correlation of Martin and Nilles [95] (see Eq. (54)).

$$\alpha_{wall} \quad \left(1.3 + 5 \cdot \frac{d_P}{d_{tube}}\right) \cdot \frac{\lambda_{bed}}{d_P} + 0.19 \cdot \frac{\lambda_G}{d_P} \cdot Re_0^{0.75} \cdot Pr^{0.33} \tag{54}$$

Re_0 is the Reynolds number defined for a catalyst particle (see Eq. (55)):

$$Re_0 \quad \frac{u_G \cdot \rho_G \cdot d_P}{\mu_G} \tag{55}$$

and *Pr* is the Prandtl number defined according to Eq. (56).

$$Pr \quad \frac{\mu_G \cdot c_{p,G}}{\lambda_G} \tag{56}$$

D Dibenzyltoluene properties

Dibenzyltoluene properties are as following [99].
Boiling range at 1013 mbar: ca. 385–395 °C .
Pour point: ca. 34 °C.
Flash point: ca. 200 °C.
Ignition temperature: ca. 500 °C.
Permissible heater film temperature: 350 °C.

Table 9
Dibenzyltoluene properties relevant for the design of a slurry bubble column reactor for three-phase CO_2 methanation [99].

T	ρ	c_p	λ	ν	p_v
°C	kg·m^{-3}	J·kg^{-1}·K^{-1}	W·m^{-1}·K^{-1}	m^2·s^{-1}	bar
0	1058	$1.48\cdot10^3$	0.133	$3.21\cdot10^{-4}$	
20	1044	$1.55\cdot10^3$	0.131	$4.70\cdot10^{-5}$	
100	987	$1.85\cdot10^3$	0.120	$3.10\cdot10^{-6}$	
200	915	$2.22\cdot10^3$	0.062	$9.2\cdot10^{-7}$	0.005
220	901	$2.29\cdot10^3$	0.060	$7.7\cdot10^{-7}$	0.012
240	887	$2.37\cdot10^3$	0.059	$6.5\cdot10^{-7}$	0.027
260	873	$2.44\cdot10^3$	0.057	$5.7\cdot10^{-7}$	0.054
280	858	$2.52\cdot10^3$	0.055	$5.0\cdot10^{-7}$	0.098
300	844	$2.59\cdot10^3$	0.054	$4.5\cdot10^{-7}$	0.200
320	830	$2.67\cdot10^3$	0.053	$4.0\cdot10^{-7}$	0.315
340	815	$2.74\cdot10^3$	0.051	$3.6\cdot10^{-7}$	0.560
360	801	$2.82\cdot10^3$	0.050	$3.2\cdot10^{-7}$	0.860

References

[1] UNFCCC, Adoption of the paris agreement. http://unfccc.int/resource/docs/2015/cop21/eng/l09r01.pdf, 2015.

[2] M. Bailera, P. Lisbona, L.M. Romeo, S. Espatolero, Power to gas projects review: lab, pilot and demo plants for storing renewable energy and co2, Renew. Sustain. Energy Rev. 69 (2017) 292 312, https://doi.org/10.1016/j.rser.2016.11.130.

[3] M. Gotz, J. Lefebvre, F. Mors, A. McDaniel Koch, F. Graf, S. Bajohr, R. Reimert, T. Kolb, Renewable power-to-gas: a technological and economic review, Renew. Energy 85 (2016) 1371 1390, https://doi.org/10.1016/j.renene.2015.07.066.

[4] M. Sterner, I. Stadler, Energiespeicher - Bedarf, Technologien, Integration, SpringerLink : Bücher, Springer Vieweg, Berlin, 2014.

[5] K. Hashimoto, N. Kumagai, K. Izumiya, H. Takano, Z. Kato, The production of renewable energy in the form of methane using electrolytic hydrogen generation, Energy Sustain. Soc. 4 (1) (2014), https://doi.org/10.1186/s13705-014-0017-5.

[6] S. Ronsch, S. Matthischke, M. Müller, P. Eichler, Dynamische simulation von reaktoren zur festbettmethanisierung: dynamic simulation of fixed-bed methanation reactors, Chem. Ing. Tech. 86 (8) (2014) 1198 1204, https://doi.org/10.1002/cite.201300046.

[7] R. Otten, Das audi e-gas-projekt: die energiewende im cng-tank, in: Erdgas Mobil Symposium, Audi AG, Berlin, 2013.

[8] J. de Swart, R. Krishna, Simulation of the transient and steady state behaviour of a bubble column slurry reactor for fischer tropsch synthesis, Chem. Eng. Process: Process Intensification 41 (1) (2002) 35 47, https://doi.org/10.1016/S0255-2701(00)00159-8.

[9] O. M. Basha, L. Sehabiague, A. Abdel-Wahab, B. I. Morsi, Fischer tropsch synthesis in slurry bubble column reactors: experimental investigations and modeling a review: Review, Int. J. Chem. React. Eng. 13 (3). doi:10.1515/ijcre-2014-0146.

[10] C.N. Satterfield, G.A. Huff, 25 effects of mass transfer on fischertropsch synthesis in slurry reactors, in: 17th International Symposium of Chemical Reaction Engineering (IS CRE 17), 35, 1980, pp. 195 202, https://doi.org/10.1016/0009-2509(80)80087-X, 1.

[11] W.D. Deckwer, Y. Serpemen, M. Ralek, B. Schmidt, On the relevance of mass transfer limitations in the fischer-tropsch slurry process, in: 17th International Symposium of Chemical Reaction Engineering (IS CRE 17), 36, 1981, pp. 773 774, https://doi.org/10.1016/0009-2509(81)85092-0, 4.

[12] D.B. Bukur, Some comments on models for fischer-tropsch reaction in slurry bubble column reactors, in: 17th International Symposium of Chemical Reaction Engineering (IS CRE 17), 38, 1983, pp. 440 446, https://doi.org/10.1016/0009-2509(83)80161-4, 3.

[13] D. Stern, A.T. Bell, H. Heinemann, Effects of mass transfer on the performance of slurry reactors used for fischer-tropsch synthesis, in: 17th International Symposium of Chemical Reaction Engineering (IS CRE 17), vol. 38, 1983, pp. 597 605, https://doi.org/10.1016/0009-2509(83)80119-5, 4.

[14] C. Maretto, R. Krishna, Modelling of a bubble column slurry reactor for fischer tropsch synthesis, Catal. Today 52 (2 3) (1999) 279 289, https://doi.org/10.1016/s0920-5861(99)00082-6.

[15] G.P. van der Laan, A.A.C.M. Beenackers, R. Krishna, Multicomponent reaction engineering model for fe-catalyzed fischer tropsch synthesis in commercial scale slurry bubble column reactors, Chem. Eng. Sci. 54 (21) (1999) 5013 5019, https://doi.org/10.1016/s0009-2509(99)00225-0.

[16] H.-S. Song, D. Ramkrishna, S. Trinh, R.L. Espinoza, H. Wright, Multiplicity and sensitivity analysis of fischer tropsch bubble column slurry reactors: plug-flow gas and well-mixed slurry model, in: 17th International Symposium of Chemical Reaction Engineering (IS CRE 17), vol. 58, 2003, pp. 2759 2766, 12.

[17] H.-S. Song, D. Ramkrishna, S. Trinh, H. Wright, Operating strategies for fischer-tropsch reactors: a model-directed study, Korean J. Chem. Eng. 21 (2) (2004) 308 317, https://doi.org/10.1007/BF02705414.

[18] F.A.N. Fernandes, Modeling and product grade optimization of fischer−tropsch synthesis in a slurry reactor, Ind. Eng. Chem. Res. 45 (3) (2006) 1047 1057, https://doi.org/10.1021/ie0507732.

[19] Y. Wang, W. Fan, Y. Liu, Z. Zeng, X. Hao, M. Chang, C. Zhang, Y. Xu, H. Xiang, Y. Li, Modeling of the fischer tropsch synthesis in slurry bubble column reactors, Chem. Eng. Process: Process Intensification 47 (2) (2008) 222 228, https://doi.org/10.1016/j.cep.2007.02.011.

[20] R. Guettel, T. Turek, Comparison of different reactor types for low temperature fischer tropsch synthesis: a simulation study, in: 17th International Symposium of Chemical Reaction Engineering (IS CRE 17), 64, 2009, pp. 955 964, https://doi.org/10.1016/j.ces.2008.10.059, 5.

[21] W.D. Deckwer, Y. Serpemen, M. Ralek, B. Schmidt, Modeling the fischer-tropsch synthesis in the slurry phase, Ind. Eng. Chem. Process Des. Dev. 21 (2) (1982) 231 241.

[22] D. Stern, A.T. Bell, H. Heinemann, A theoretical model for the performance of bubble-column reactors used for fischertropsch synthesis, in: 17th International Symposium of Chemical Reaction Engineering (IS CRE 17), vol. 40, 1985, pp. 1665 1677, https://doi.org/10.1016/0009-2509(8580027-0), 9.

[23] J.R. Turner, P.L. Mills, Comparison of axial dispersion and mixing cell models for design and simulation of fischer-tropsch slurry bubble column reactors, in: 17th International Symposium of Chemical Reaction Engineering (IS CRE 17), vol. 45, 1990, pp. 2317 2324, https://doi.org/10.1016/0009-2509(90)80111-Q, 8.

[24] A. Prakash, On the effects of syngas composition and water-gas-shift reaction rate on ft synthesis over iron based catalyst in a slurry reactor, Chem. Eng. Commun. 128 (1) (1994) 143 158.

[25] N. Rados, M.H. Al-Dahhan, M.P. Dudukovic, Modeling of the fischer tropsch synthesis in slurry bubble column reactors, Catal. Today 79 80 (2003) 211 218, https://doi.org/10.1016/S0920-5861(03)00007-5.

[26] N. Rados, M.H. Al-Dahhan, M.P. Dudukovĭc, Dynamic modeling of slurry bubble column reactors, Ind. Eng. Chem. Res. 44 (16) (2005) 6086 6094, https://doi.org/10.1021/ie040227t.

[27] L. Sehabiague, R. Lemoine, A. Behkish, Y.J. Heintz, M. Sanoja, R. Oukaci, B.I. Morsi, Modeling and optimization of a large-scale slurry bubble column reactor for producing 10,000 bbl/day of fischer tropsch liquid hydrocarbons: festschrift issue in honor of professor shiao-hung chiang, J. Chin. Inst. Chem. Eng. 39 (2) (2008) 169 179, https://doi.org/10.1016/j.jcice.2007.11.003.

[28] S. Seyednejadian, R. Rauch, S. Bensaid, H. Hofbauer, G. Weber, G. Saracco, Power to fuels: dynamic modeling of a slurry bubble column reactor in lab-scale for fischer tropsch synthesis under variable load of synthesis gas, Appl. Sci. 8 (4). doi:10.3390/app8040514.

[29] K. Rietema, Science and technology of dispersed two-phase systems i and ii, in: 17th International Symposium of Chemical Reaction Engineering (IS CRE 17), vol. 37, 1982, pp. 1125 1150, https://doi.org/10.1016/0009-2509(82)85058-6, 8.

[30] P. Zehner, Impuls-, stoff- und warmetransport in blasensaulen, Chem. Ing. Tech. 54 (3) (1982) 248 251, https://doi.org/10.1002/cite.330540311.

[31] K.G. Anderson, R.G. Rice, Local turbulence model for predicting circulation rates in bubble columns, AIChE J. 35 (3) (1989) 514 518, https://doi.org/10.1002/aic.690350321.

[32] H.-E. Gasche, C. Edinger, H. Kompel, H. Hofmann, Hydrodynamics in bubble columns, Chem. Eng. Process: Process Intensification 26 (2) (1989) 101 109, https://doi.org/10.1016/0255-2701(89)90002-0.

[33] N.N. Clark, J.W. van Egmond, E.P. Nebiolo, The driftflux model applied to bubble columns and low velocity flows, Int. J. Multiph. Flow 16 (2) (1990) 261 279, https://doi.org/10.1016/0301-9322(90)90058-Q.

[34] R.G. Rice, N.W. Geary, Prediction of liquid circulation in viscous bubble columns, AIChE J. 36 (9) (1990) 1339 1348, https://doi.org/10.1002/aic.690360907.

[35] N.W. Geary, R.G. Rice, Circulation in bubble columns: corrections for distorted bubble shape, AIChE J. 37 (10) (1991) 1593 1594, https://doi.org/10.1002/aic.690371018.

[36] N.W. Geary, R.G. Rice, Circulation and scale-up in bubble columns, AIChE J. 38 (1) (1992) 76 82, https://doi.org/10.1002/aic.690380108.

[37] J. Grienberger, H. Hofmann, Investigations and modelling of bubble columns, in: 17th International Symposium of Chemical Reaction Engineering (IS CRE 17), vol. 47, 1992, pp. 2215 2220, https://doi.org/10.1016/0009-2509(92)87037-Q, 9.

[38] H.F. Svendsen, H.A. Jakobsen, R. Torvik, Local flow structures in internal loop and bubble column reactors, in: 17th International Symposium of Chemical Reaction Engineering (IS CRE 17), 47, 1992, pp. 3297 3304, https://doi.org/10.1016/0009-2509(92)85038-D, 13.

[39] V.V. Ranade, Flow in bubble columns: some numerical experiments, in: 17th International symposium of chemical reaction engineering (IS CRE 17), 47, 1992, pp. 1857 1869, https://doi.org/10.1016/0009-2509(92)80304-U, 8.

[40] A. Sokolichin, G. Eigenberger, Gas liquid flow in bubble columns and loop reactors: Part i. detailed modelling and numerical simulation, in: 17th International Symposium of Chemical Reaction Engineering (IS CRE 17), 49, 1994, pp. 5735 5746, https://doi.org/10.1016/0009-2509(94)00289-4, 24.

[41] M. Millies, D. Mewes, Calculation of circulating flows in bubble columns, in: 17th International symposium of chemical reaction engineering (IS CRE 17), 50, 1995, pp. 2093 2106, https://doi.org/10.1016/0009-2509(94)00500-Q,

13.
[42] E. Delnoij, J. Kuipers, W. van Swaaij, Dynamic simulation of gas-liquid two-phase flow: effect of column aspect ratio on the flow structure, in: 17th International Symposium of Chemical Reaction Engineering (IS CRE 17), 52, 1997, pp. 3759 3772, https://doi.org/10.1016/S0009-2509(97)00222-4, 21.
[43] E. Delnoij, F.A. Lammers, J. Kuipers, W. van Swaaij, Dynamic simulation of dispersed gas-liquid two-phase flow using a discrete bubble model, in: 17th International Symposium of Chemical Reaction Engineering (IS CRE 17), 52, 1997, pp. 1429 1458, https://doi.org/10.1016/S0009-2509(96)00515-5, 9.
[44] S. Grevskott, B.H. Sannæs, M.P. Dudukovic, K.W. Hjarbo, H.F. Svendsen, Liquid circulation, bubble size distributions, and solids movement in two- and three-phase bubble columns, in: 17th International Symposium of Chemical Reaction Engineering (IS CRE 17), 51, 1996, pp. 1703 1713, https://doi.org/10.1016/0009-2509(96)00029-2, 10.
[45] D. Mitra-Majumdar, B. Farouk, Y.T. Shah, Hydrodynamic modeling of three-phase flows through a vertical column, in: 17th International symposium of chemical reaction engineering (IS CRE 17), 52, 1997, pp. 4485 4497, https://doi.org/10.1016/S0009-2509(97)00293-5, 24.
[46] W. Jianping, X. Shonglin, Local hydrodynamics in a gas-liquid-solid three-phase bubble column reactor, in: Catalytic Reaction and Reactor Engineering EuropaCat V Limerick, Sept 2-7 2001, vol. 70, 1998, pp. 81 84, https://doi.org/10.1016/S1385-8947(97)00120-4, 1.
[47] N.T. Padial, W.B. VanderHeyden, R.M. Rauenzahn, S.L. Yarbro, Three-dimensional simulation of a three-phase draft-tube bubble column, in: 17th International Symposium of Chemical Reaction Engineering (IS CRE 17), vol. 55, 2000, pp. 3261 3273, https://doi.org/10.1016/S0009-2509(99)00587-4, 16.
[48] D. Matonis, D. Gidaspow, M. Bahary, Cfd simulation of flow and turbulence in a slurry bubble column, AIChE J. 48 (7) (2002) 1413 1429, https://doi.org/10.1002/aic.690480706.
[49] V. Michele, D.C. Hempel, Liquid flow and phase holdup measurement and cfd modeling for two-and three-phase bubble columns, Chem. Eng. Sci. 57 (11) (2002) 1899 1908, https://doi.org/10.1016/S0009-2509(02)00051-9.
[50] M.R. Rampure, V.V. Buwa, V.V. Ranade, Modelling of gasliquid/gas-liquid-solid flows in bubble columns: experiments and cfd simulations, Can. J. Chem. Eng. 81 (3 4) (2003) 692 706, https://doi.org/10.1002/cjce.5450810348.
[51] I.K. Gamwo, J.S. Halow, D. Gidaspow, R. Mostofi, Cfd models for methanol synthesis three-phase reactors: reactor optimization, in: Catalytic Reaction and Reactor Engineering EuropaCat V Limerick, Sept 2-7 2001, vol. 93, 2003, pp. 103 112, https://doi.org/10.1016/S1385-8947(02)00192-4, 2.
[52] G. Cartland Glover, S. Generalis, Gas liquid solid flow modelling in a bubble column, Chem. Eng. Process: Process Intensification 43 (2) (2004) 117 126, https://doi.org/10.1016/S0255-2701(03)00009-6.
[53] W. Feng, J. Wen, J. Fan, Q. Yuan, X. Jia, Y. Sun, Local hydrodynamics of gas liquid-nanoparticles three-phase fluidization, in: 17th International Symposium of Chemical Reaction Engineering (IS CRE 17), vol. 60, 2005, pp. 6887 6898, https://doi.org/10.1016/j.ces.2005.06.006, 24.
[54] D. Wiemann, D. Mewes, Calculation of flow fields in two and threephase bubble columns considering mass transfer, in: 17th InternationalSymposium of Chemical Reaction Engineering (IS CRE 17), vol. 60, 2005, pp. 6085 6093, https://doi.org/10.1016/j.ces.2005.04.054, 22.
[55] J. Schallenberg, J.H. Enß, D.C. Hempel, The important role of local dispersed phase hold-ups for the calculation of three-phase bubble columns, Chem. Eng. Sci. 60 (22) (2005) 6027 6033, https://doi.org/10.1016/j.ces.2005.02.017.
[56] K.-T. Nguyen, S.-C. Huang, Simulation of hydrodynamic characteristics of glass beads in gas-liquid-solid three phase fluidized beds by computational fluid dynamics, J. Eng. Technol. Educ. (2) (2007) 248 261.
[57] R. Panneerselvam, S. Savithri, G.D. Surender, Cfd simulation of hydrodynamics of gas liquid solid fluidised bed reactor, in: 17th International Symposium of Chemical Reaction Engineering (IS CRE 17), vol. 64, 2009, pp. 1119 1135, https://doi.org/10.1016/j.ces.2008.10.052, 6.
[58] P. Muthiah, K. Ponnusamy, T.K. Radhakrishnan, Cfd modeling of flow pattern and phase holdup of three phase fluidized bed contactor, Chem. Prod. Process Model. 4 (1) (2009) 36.
[59] P.J. O'Rourke, P. Zhao, D. Snider, A model for collisional exchange in gas/liquid/solid fluidized beds, in: 17th International Symposium of Chemical Reaction Engineering (IS CRE 17), vol. 64, 2009, pp. 1784 1797, https://doi.org/10.1016/j.ces.2008.12.014, 8.
[60] A.A. Troshko, F. Zdravistch, Cfd modeling of slurry bubble column reactors for Fisher tropsch synthesis, Chem. Eng. Sci. 64 (5) (2009) 892 903, https://doi.org/10.1016/j.ces.2008.10.022.
[61] K. Sivaguru, K.M.S. Begum, N. Anantharaman, Hydrodynamic studies on three-phase fluidized bed using cfd analysis, in: Catalytic Reaction and Reactor Engineering EuropaCat V Limerick, Sept 2-7 2001, vol. 155, 2009, pp. 207 214, https://doi.org/10.1016/j.cej.2009.07.037, 1 2.
[62] E.M. Matos, R. Guirardello, M. Mori, J.R. Nunhez, Modeling and simulation of a pseudo-three-phase slurry bubble column reactor applied to the process of petroleum hydrodesulfurization, Comput. Chem. Eng. 33 (6) (2009) 1115 1122, https://doi.org/10.1016/j.compchemeng.2008.12.011.
[63] M. Hamidipour, J. Chen, F. Larachi, Cfd study on hydrodynamics in three-phase fluidized beds application of turbulence models and experimental validation, in: 17th International Symposium of Chemical Reaction Engineering (IS CRE 17), 78, 2012, pp. 167 180, https://doi.org/10.1016/j.ces.2012.05.016.
[64] B.O. M, W. Li, M. Zhuowu, M.B. I, Cfd Modeling with Experimental Validation of the Internal Hydrodynamics in a Pilot-Scale Slurry Bubble Column Reactor, 2016, https://doi.org/10.1515/ijcre-2015-0165.
[65] Y. Li, J. Zhang, L.-S. Fan, Numerical simulation of gas liquid solid fluidization systems using a combined cfd-vof-dpm method: bubble wake behavior, in: 17th International Symposium of Chemical Reaction Engineering (IS CRE 17), vol. 54, 1999, pp. 5101 5107, https://doi.org/10.1016/S0009-2509(99)00263-8, 21.
[66] J. Zhang, Y. Li, L.-S. Fan, Numerical studies of bubble and particle dynamics in a three-phase fluidized bed at elevated pressures, Powder Technol. 112 (1 2) (2000) 46 56, https://doi.org/10.1016/S0032-5910(99)00304-6.
[67] J. Zhang, Y. Li, L.-S. Fan, Discrete phase simulation of gas liquid solid fluidization systems: single bubble rising behavior, Powder Technol. 113 (3) (2000) 310 326, https://doi.org/10.1016/S0032-5910(00)00314-4.
[68] C. Chen, L.-S. Fan, Discrete simulation of gas-liquid bubble columns and gas-liquid-solid fluidized beds, AIChE J. 50 (2) (2004) 288 301, https://doi.org/10.1002/aic.10027.
[69] M. van Sint Annaland, N.G. Deen, J. Kuipers, Numerical simulation of gas bubbles behaviour using a three-dimensional volume of fluid method, in: 17th International Symposium of Chemical Reaction Engineering (IS CRE 17), vol. 60, 2005, pp. 2999 3011, https://doi.org/10.1016/j.ces.2005.01.031, 11.
[70] X. Zhang, G. Ahmadi, Eulerian Lagrangian simulations of liquid gas solid flows in three-phase slurry reactors, in: 17th International Symposium of Chemical Reaction Engineering (IS CRE 17), vol. 60, 2005, pp. 5089 5104, https://doi.org/10.1016/j.ces.2005.04.033, 18.
[71] C. Cao, M. Liu, J. Wen, Q. Guo, Experimental measurement and numerical simulation for liquid flow velocity and local phase hold-ups in the riser of a glscfb, Chem. Eng. Process: Process Intensification 48 (2009) 288 295, https://doi.org/10.1016/j.cep.2008.04.004, 1.
[72] E. Tsotsas, M7 warmeleitung und dispersion in durchstromten schüttungen, in: VDI-Warmeatlas, Springer Berlin Heidelberg, Berlin, Heidelberg, 2013, pp. 1517 1534, https://doi.org/10.1007/978-3-642-19981-3_102.
[73] D.E. Mears, Tests for transport limitations in experimental catalytic reactors, Ind. Eng. Chem. Process Des. Dev. 10 (4) (1971) 541 547, https://doi.org/10.1021/i260040a020.
[74] J.B.A. Anderson, Criterion for isothermal behaviour of a catalyst pellet, Chem. Eng. Sci. 18 (1963) 147.
[75] E.W. Thiele, Relation between catalytic activity and size of particle, Ind. Eng. Chem. 31 (7) (1939) 916 920, https://doi.org/10.1021/ie50355a027.
[76] D. Schlereth, O. Hinrichsen, A fixed-bed reactor modeling study on the methanation of co2, ECCE9 9th Eur. Congr. Chem. Eng. 92 (4) (2014) 702 712, https://doi.org/10.1016/j.cherd.2013.11.014.
[77] D. Sun, D.S. Simakov, Thermal management of a sabatier reactor for co2 conversion into ch4: simulation-based analysis, J. CO2 Util. 21 (Supplement C) (2017) 368 382, https://doi.org/10.1016/j.jcou.2017.07.015.
[78] D. Sun, F.M. Khan, D.S. Simakov, Heat removal and catalyst deactivation in a sabatier reactor for chemical fixation of co2: simulationbased analysis, in: Catalytic Reaction and Reactor Engineering EuropaCat V Limerick, Sept 2-7 2001, vol. 329, 2017, pp. 165 177, https://doi.org/10.1016/j.cej.2017.06.160 (Supplement C).
[79] M. Gotz, F. Graf, J. Lefebvre, S. Bajohr, R. Reimert, Speicherung elektrischer energie aus regenerativen quellen im erdgasnetz arbeitspaket 5: Betrachtungen des gesamtsystems im hinblick auf dynamik und prozessintegration, Energ. Wasser Prax. 65 (11) (2014) 51 55.
[80] M. Gotz, J. Lefebvre, F. Mors, R. Reimert, F. Graf, T. Kolb, Hydrodynamics of organic and ionic liquids in a slurry bubble column reactor operated at elevated temperatures, Chem. Eng. J. 286 (2016) 348 360, https://doi.org/10.1016/j.cej.2015.10.044.
[81] M. Gotz, Methanisierung im dreiphasen-reaktor, Ph.D. thesis, Karlsruher Institut für Technologie (KIT), Karlsruhe, 2014.
[82] A. Behkish, R. Lemoine, R. Oukaci, B.I. Morsi, Novel correlations for gas holdup in large-scale slurry bubble column reactors operating under elevated pressures and temperatures, Chem. Eng. J. 115 (3) (2006) 157 171, https://doi.org/10.1016/j.cej.2005.10.006.
[83] R. Lemoine, A. Behkish, L. Sehabiague, Y.J. Heintz, R. Oukaci, B.I. Morsi, An algorithm for predicting the hydrodynamic and mass transfer parameters in bubble column and slurry bubble column reactors, Fuel Process. Technol. 89 (4) (2008) 322 343, https://doi.org/10.1016/j.fuproc.2007.11.016.
[84] T. Reith, S. Renken, B.A. Israel, Gas hold-up and axial mixing in the fluid phase of bubble columns, in: 17th International Symposium of Chemical Reaction Engineering (IS CRE 17), vol. 23, 1968, pp. 619 629, https://doi.org/10.1016/0009-2509(68)89007-4, 6.
[85] Y. Ohki, H. Inoue, Longitudinal mixing of the liquid phase in bubble columns, in: 17th International Symposium of Chemical Reaction Engineering (IS CRE 17), vol. 25, 1970, pp. 1 16, https://doi.org/10.1016/0009-2509(70)85016-3, 1.
[86] Y. Kato, Longitudinal dispersion coefficient of a liquid in a bubble column, Int. Chem. Eng. 12 (1) (1972) 182 187.
[87] G.D. Towell, G.H. Ackerman (Eds.), Axial Mixing of Liquid and Gas in Large Bubble Reactors, 1972.
[88] K. Akita, F. Yoshida, Gas holdup and volumetric mass transfer coefficient in bubble columns. effects of liquid properties, Ind. Eng. Chem. Process Des. Dev. 12 (1) (1973) 76 80, https://doi.org/10.1021/i260045a015.
[89] R. Badura, W.-D. Deckwer, H.-J. Warnecke, H. Langemann, Durchmischung in

blasensaulen, Chem. Ing. Tech. 46 (9) (1974) 399, https://doi.org/10.1002/cite.330460909.
[90] H. Hikita, H. Kikukawa, Liquid-phase mixing in bubble columns: effect of liquid properties, Chem. Eng. J. 8 (3) (1974) 191 197, https://doi.org/10.1016/0300-9467(74)85024-0.
[91] W.-D. Deckwer, R. Burckhart, G. Zoll, Mixing and mass transfer in tall bubble columns, in: 17th International Symposium of Chemical Reaction Engineering (IS CRE 17), vol. 29, 1974, pp. 2177 2188, https://doi.org/10.1016/0009-2509(74)80025-4, 11.
[92] J. Lefebvre, N. Trudel, S. Bajohr, T. Kolb, A study on three-phase co2 methanation reaction kinetics in a continuous stirred-tank slurry reactor, Fuel 217 (2018) 151 159, https://doi.org/10.1016/j.fuel.2017.12.082.
[93] W.-D. Deckwer, On the mechanism of heat transfer in bubble column reactors, in: 17th International Symposium of Chemical Reaction Engineering (IS CRE 17), vol. 35, 1980, pp. 1341 1346, https://doi.org/10.1016/0009-2509(80)85127-X, 6.
[94] J. Lefebvre, S. Bajohr, T. Kolb, A comparison of two-phase and three-phase co2 methanation reaction kinetics, Fuel 239 (2019) 896 904, https://doi.org/10.1016/j.fuel.2018.11.051.
[95] H. Martin, M. Nilles, Radiale warmeleitung in durchstromten schüttungsrohren, Chem. Ing. Tech. 65 (12) (1993) 1468 1477, https://doi.org/10.1002/cite.330651206.
[96] S. Ergun, Fluid flow through packed columns, Chem. Eng. Prog. 48 (1952) 89 94.
[97] N.G. Deen, R.F. Mudde, J. Kuipers, P. Zehner, M. Kraume, Bubble columns, in: Ullmann's Encyclopedia of Industrial Chemistry, Wiley-VCH Verlag GmbH & Co. KGaA, Weinheim, Germany, 2000, https://doi.org/10.1002/14356007.b04_275.pub2.
[98] S. Nedeltchev, A. Schumpe, Slurry reactors, in: Handbook of Heterogeneous Catalysis, Wiley-VCH Verlag GmbH & Co. KGaA, 2008, https://doi.org/10.1002/9783527610044.hetcat0113.
[99] Sasol GmbH, Marlotherm Sh Product Information, 2014.
[100] A. Sauciuc, Z. Abosteif, G. Weber, A. Potetz, R. Rauch, H. Hofbauer, G. Schaub, L. Dumitrescu, Influence of operating conditions on the performance of biomass-based fischer tropsch synthesis, Biomass Convers. Biorefinery 2 (3) (2012) 253 263, https://doi.org/10.1007/s13399-012-0060-4.
[101] M. Baerns, H. Hofmann, A. Renken, Chemische Reaktionstechnik: Lehrbuch der Technischen Chemie, third ed., 1999. Thieme, Stuttgart and, New York.
[102] P.B. Weisz, C.D. Prater, Interpretation of measurements in experimental catalysis, Adv. Catal. 6 (1954) 143 196, https://doi.org/10.1016/S0360-0564(08)60390-9.
[103] M. Kleiber, R. Joh, D3 stoffwerte von sonstigen reinen fluiden, in: VDI Warmeatlas, Springer Berlin Heidelberg, Berlin, Heidelberg, 2013, pp. 357 488, https://doi.org/10.1007/978-3-642-19981-3_20.
[104] M. Kleiber, R. Joh, Da1 berechnungsmethoden für stoffeigenschaften, in: VDI-Warmeatlas, Springer Berlin Heidelberg, Berlin, Heidelberg, 2006, pp. 103 132, https://doi.org/10.1007/978-3-540-32218-4_10.
[105] S.C. Saxena, N.S. Rao, A.C. Saxena, Heat-transfer and gas-holdup studies in a bubble column: air-water-glass bead system, Chem. Eng. Commun. 96 (1) (1990) 31 55.
[106] C.R. Wilke, P. Chang, Correlation of diffusion coefficients in dilute solutions, AIChE J. 1 (2) (1955) 264 270, https://doi.org/10.1002/aic.690010222.
[107] W.-D. Deckwer, Reaktionstechnik in Blasensaulen, first ed., Grundlagen der chemischen Technik, Salle and Sauerlander, Frankfurt am Main and Aarau, 1985.